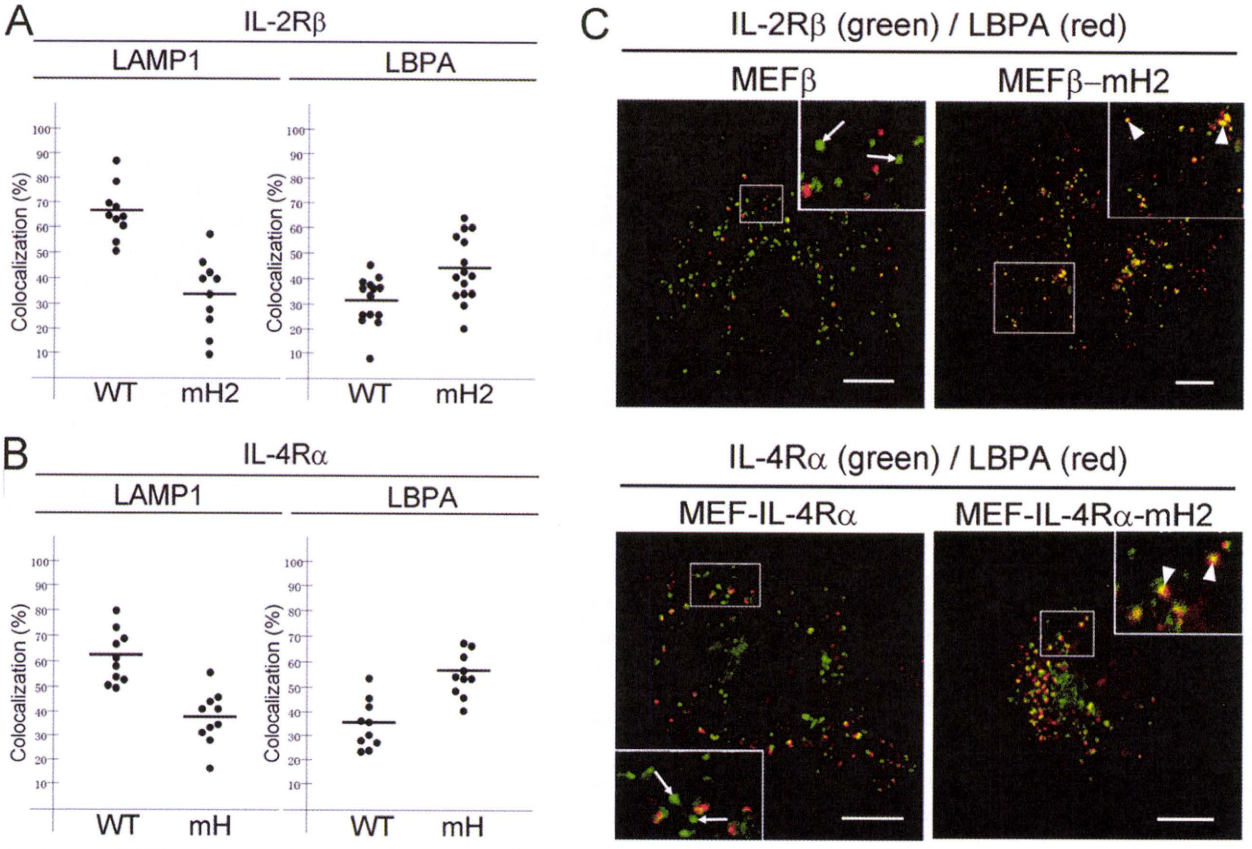

FIGURE 9. **Localizations of IL-2Rβ and IL-4Rα mutants lacking the hydrophobic amino acid cluster to LBPA-positive compartments.** MEF transfectants were grown on coverslips, fixed, and double-labeled with an anti-IL-2Rβ antibody (C20) or anti-IL-4Rα antibody (C20) and an anti-LAMP1 monoclonal antibody or anti-LBPA monoclonal antibody. Fluorescence images of the MEF transfectants ($n \geq 10$ cells) were captured using a confocal laser microscope. The percentages of the IL-2Rβ-positive (*A*) and IL-4Rα-positive (*B*) pixel areas that were colocalized with LAMP1 (*left*) and LBPA (*right*) were analyzed. *C*, the IL-2Rβ-positive and IL-4Rα-positive pixel areas that were colocalized with LBPA (*arrowheads*) and not with LBPA (*arrows*) are indicated. Fluorescence labeling was carried out for IL-2Rβ (*green*), IL-4Rα (*green*), and LBPA (*red*). *Scale bars*, 10 μm.

ing compartments, similar to *YXXϕ* signal sequences. For example, the (D/E)*XXX*L(L/I) signal sequence in the CD3-γ chain mediates its rapid internalization and lysosomal targeting (43), and internalization of glucose transporter 8 is mediated by the interaction of (D/E)*XXX*L(L/I) signal sequence with AP2 complex (44), indicating that (D/E)*XXX*L(L/I) signal sequence plays a essential role for the internalization in the membrane proteins. In contrast, the hydrophobic amino acid clusters found in this study were involved in the interaction with Hrs and not needed for the internalization of the receptors. Another type of dileucine-based signal sequence (D*XX*LL) is present in molecules at the plasma membrane, trans-Golgi network, and endosomes and is recognized by another family of adaptor proteins known as Golgi-localized γ-ear-containing Arf-binding proteins (GGAs). The D*XX*LL sequence interacts with the VHS domain of GGAs (45, 46). On the other hand, the VHS domains of both Hrs and STAM bind to ubiquitin but not the D*XX*LL sequence (45, 47). Regarding other signal sequences, acidic amino acid clusters are present in some transmembrane proteins and are considered to play roles in their retrieval from endosomes to the trans-Golgi network (1). The hydrophobic amino acid cluster identified in this study is unique in the following points; (i) the cluster is involved in ubiquitin-independent sorting (ii) the cluster is recognized by Hrs, a known sorting component of the ubiquitin-dependent machinery ESCRT-0, and (iii) the cluster comprises FFFHL in IL-2Rβ and LFLDLL in IL-4Rα, indicating that the amino acid sequence of the cluster may vary a great deal. Thus, we speculate that Hrs may recognize the hydrophobic amino acid clusters in various receptors with broad specificity. In this regard, our analyses to identify a key domain (amino acids 428–466) in Hrs that influences the receptor binding are important. Although there is no motif involved in the protein-protein interaction, we focused on a hydrophobic amino acid cluster comprising amino acids 453–457 (LLELL) in the C-terminal half of Hrs. We generated an Hrs mutant with the hydrophobic amino acids (residues 453–457) with alanine and examined the binding between this Hrs mutant and IL-2Rβ or IL-4Rα. Only slight reductions in the associations of the Hrs mutant with the receptors were observed (data not shown). Accordingly, extensive analyses, including solution of the crystallographic structure, will be needed to explore this region (amino acids 428–466) of Hrs. Recently, the complete crystal structure of human ESCRT-0 core complex was clarified (48). Analyses of the crystal structure revealed that the coiled-coil domains of Hrs and STAM form an antiparallel two-stranded coiled-coil. The coiled-coil domain of Hrs consists of four α-helix strands, α1 (amino acids 406–429), α2 (amino acids 432–436), α3-N (amino acids 437–

453), and α3-C (amino acids 470–498). Because the hydrophobic amino acid cluster binding region (residues 428–466) of Hrs includes the hinge region between α1 and α2, the area around the hinge region may be a candidate site that contributes to the interaction.

On the other hand, what are the biological features of the receptors that are recognized by Hrs in a ubiquitin-independent manner? The epidermal growth factor receptor is localized on the cell surface membrane in the absence of ligand stimulation, and receptor internalization and transport to the MVB pathway are initiated following receptor ubiquitylation after ligand stimulation (49–52). In contrast, IL-2Rβ is constitutively internalized and delivered to the lysosomal pathway in the absence of its ligand (23). We found that IL-4Rα as well as IL-2Rβ was localized to LAMP1-positive compartments without ligand stimulation, suggesting constitutive internalization and endosomal sorting of IL-4Rα. Consequently, we speculate that the ubiquitin-independent binding targets of Hrs may be certain kinds of receptors that have the properties of constitutive internalization and sorting to lysosomes.

In conclusion, ESCRT complexes including ESCRT-0, which consists of Hrs and STAM, serve as the transport machinery for ubiquitylated cargo proteins. Therefore, it is noteworthy that Hrs associates with cytokine receptors in a ubiquitin-independent manner and is involved in their transport during endosomal sorting. In the present study we found that Hrs recognized a hydrophobic amino acid cluster in two cytokine receptors and played a role in the precise delivery of the receptors to late endosomes. These findings suggest the existence of a group of cargo proteins that are independent of ubiquitylation for endosomal sorting and have the hydrophobic amino acid cluster as an endosomal sorting signal motif.

Acknowledgments—We thank Dr. T. Kobayashi (RIKEN Advanced Science Institute, Saitama, Japan) for providing the anti-LBPA antibody, Dr. K. Miyazono (The University of Tokyo) for providing the pcDNA-HA-ubiquitin, and Dr. T. Kitamura (The University of Tokyo) for providing the pMXs. We also thank the Instrumental Analysis Research Center for Human and Environmental Sciences at Shinshu University for technical assistance with the DNA sequencing, flow cytometry analyses, and confocal microscopy.

REFERENCES

1. Bonifacino, J. S., and Traub, L. M. (2003) *Annu. Rev. Biochem.* **72,** 395–447
2. Di Fiore, P. P., Polo, S., and Hofmann, K. (2003) *Nat. Rev. Mol. Cell. Biol.* **4,** 491–497
3. Hicke, L., Schubert, H. L., and Hill, C. P. (2005) *Nat. Rev. Mol. Cell. Biol.* **6,** 610–621
4. Katzmann, D. J., Babst, M., and Emr, S. D. (2001) *Cell* **106,** 145–155
5. Alam, S. L., Sun, J., Payne, M., Welch, B. D., Blake, B. K., Davis, D. R., Meyer, H. H., Emr, S. D., and Sundquist, W. I. (2004) *EMBO J.* **23,** 1411–1421
6. Slagsvold, T., Aasland, R., Hirano, S., Bache, K. G., Raiborg, C., Trambaiolo, D., Wakatsuki, S., and Stenmark, H. (2005) *J. Biol. Chem.* **280,** 19600–19606
7. Hanson, P. I., Roth, R., Lin, Y., and Heuser, J. E. (2008) *J. Cell Biol.* **180,** 389–402
8. Lata, S., Schoehn, G., Jain, A., Pires, R., Piehler, J., Gottlinger, H. G., and Weissenhorn, W. (2008) *Science* **321,** 1354–1357
9. Teis, D., Saksena, S., and Emr, S. D. (2008) *Dev. Cell* **15,** 578–589
10. Saksena, S., Wahlman, J., Teis, D., Johnson, A. E., and Emr, S. D. (2009) *Cell* **136,** 97–109
11. Wollert, T., Wunder, C., Lippincott-Schwartz, J., and Hurley, J. H. (2009) *Nature* **458,** 172–177
12. Komada, M., and Kitamura, N. (1995) *Mol. Cell. Biol.* **15,** 6213–6221
13. Takeshita, T., Arita, T., Asao, H., Tanaka, N., Higuchi, M., Kuroda, H., Kaneko, K., Munakata, H., Endo, Y., Fujita, T., and Sugamura, K. (1996) *Biochem. Biophys. Res. Commun.* **225,** 1035–1039
14. Asao, H., Sasaki, Y., Arita, T., Tanaka, N., Endo, K., Kasai, H., Takeshita, T., Endo, Y., Fujita, T., and Sugamura, K. (1997) *J. Biol. Chem.* **272,** 32785–32791
15. Lloyd, T. E., Atkinson, R., Wu, M. N., Zhou, Y., Pennetta, G., and Bellen, H. J. (2002) *Cell* **108,** 261–269
16. Polo, S., Sigismund, S., Faretta, M., Guidi, M., Capua, M. R., Bossi, G., Chen, H., De Camilli, P., and Di Fiore, P. P. (2002) *Nature* **416,** 451–455
17. Raiborg, C., Bache, K. G., Gillooly, D. J., Madshus, I. H., Stang, E., and Stenmark, H. (2002) *Nat. Cell Biol.* **4,** 394–398
18. Mizuno, E., Kawahata, K., Kato, M., Kitamura, N., and Komada, M. (2003) *Mol. Biol. Cell* **14,** 3675–3689
19. Raiborg, C., and Stenmark, H. (2009) *Nature* **458,** 445–452
20. Bishop, N., Horman, A., and Woodman, P. (2002) *J. Cell Biol.* **157,** 91–101
21. Shih, S. C., Katzmann, D. J., Schnell, J. D., Sutanto, M., Emr, S. D., and Hicke, L. (2002) *Nat. Cell Biol.* **4,** 389–393
22. Sugamura, K., Asao, H., Kondo, M., Tanaka, N., Ishii, N., Ohbo, K., Nakamura, M., and Takeshita, T. (1996) *Annu. Rev. Immunol.* **14,** 179–205
23. Yamashita, Y., Kojima, K., Tsukahara, T., Agawa, H., Yamada, K., Amano, Y., Kurotori, N., Tanaka, N., Sugamura, K., and Takeshita, T. (2008) *J. Cell Sci.* **121,** 1727–1738
24. Takeshita, T., Asao, H., Ohtani, K., Ishii, N., Kumaki, S., Tanaka, N., Munakata, H., Nakamura, M., and Sugamura, K. (1992) *Science* **257,** 379–382
25. Suzuki, J., Takeshita, T., Ohbo, K., Asao, H., Tada, K., and Sugamura, K. (1989) *Int. Immunol.* **1,** 373–377
26. Tanaka, Y., Tozawa, H., Hayami, M., Sugamura, K., and Hinuma, Y. (1985) *Microbiol. Immunol.* **29,** 959–972
27. Ishii, N., Takeshita, T., Kimura, Y., Tada, K., Kondo, M., Nakamura, M., and Sugamura, K. (1994) *Int. Immunol.* **6,** 1273–1277
28. Fraker, P. J., and Speck, J. C., Jr. (1978) *Biochem. Biophys. Res. Commun.* **80,** 849–857
29. Gillooly, D. J., Raiborg, C., and Stenmark, H. (2003) *Histochem. Cell Biol.* **120,** 445–453
30. Radhakrishna, H., and Donaldson, J. G. (1997) *J. Cell Biol.* **139,** 49–61
31. Taniguchi, T., and Minami, Y. (1993) *Cell* **73,** 5–8
32. Harada, N., Yang, G., Miyajima, A., and Howard, M. (1992) *J. Biol. Chem.* **267,** 22752–22758
33. Ohbo, K., Takeshita, T., Asao, H., Kurahayashi, Y., Tada, K., Mori, H., Hatakeyama, M., Taniguchi, T., and Sugamura, K. (1991) *J. Immunol. Methods* **142,** 61–72
34. Kobayashi, T., Stang, E., Fang, K. S., de Moerloose, P., Parton, R. G., and Gruenberg, J. (1998) *Nature* **392,** 193–197
35. Matsuo, H., Chevallier, J., Mayran, N., Le Blanc, I., Ferguson, C., Fauré, J., Blanc, N. S., Matile, S., Dubochet, J., Sadoul, R., Parton, R. G., Vilbois, F., and Gruenberg, J. (2004) *Science* **303,** 531–534
36. Canfield, W. M., Johnson, K. F., Ye, R. D., Gregory, W., and Kornfeld, S. (1991) *J. Biol. Chem.* **266,** 5682–5688
37. Jadot, M., Canfield, W. M., Gregory, W., and Kornfeld, S. (1992) *J. Biol. Chem.* **267,** 11069–11077
38. Humphrey, J. S., Peters, P. J., Yuan, L. C., and Bonifacino, J. S. (1993) *J. Cell Biol.* **120,** 1123–1135
39. Williams, M. A., and Fukuda, M. (1990) *J. Cell Biol.* **111,** 955–966
40. Harter, C., and Mellman, I. (1992) *J. Cell Biol.* **117,** 311–325
41. Marks, M. S., Woodruff, L., Ohno, H., and Bonifacino, J. S. (1996) *J. Cell Biol.* **135,** 341–354
42. Chen, W. J., Goldstein, J. L., and Brown, M. S. (1990) *J. Biol. Chem.* **265,** 3116–3123
43. Letourneur, F., and Klausner, R. D. (1992) *Cell* **69,** 1143–1157
44. Schmidt, U., Briese, S., Leicht, K., Schürmann, A., Joost, H. G., and Al-Hasani, H. (2006) *J. Cell Sci.* **119,** 2321–2331

45. Puertollano, R., Aguilar, R. C., Gorshkova, I., Crouch, R. J., and Bonifacino, J. S. (2001) *Science* **292,** 1712–1716
46. Zhu, Y., Doray, B., Poussu, A., Lehto, V. P., and Kornfeld, S. (2001) *Science* **292,** 1716–1718
47. Ren, X., and Hurley, J. H. (2010) *EMBO J.* **29,** 1045–1054
48. Ren, X., Kloer, D. P., Kim, Y. C., Ghirlando, R., Saidi, L. F., Hummer, G., and Hurley, J. H. (2009) *Structure* **17,** 406–416
49. Joazeiro, C. A., Wing, S. S., Huang, H., Leverson, J. D., Hunter, T., and Liu, Y. C. (1999) *Science* **286,** 309–312
50. Levkowitz, G., Waterman, H., Ettenberg, S. A., Katz, M., Tsygankov, A. Y., Alroy, I., Lavi, S., Iwai, K., Reiss, Y., Ciechanover, A., Lipkowitz, S., and Yarden, Y. (1999) *Mol. Cell* **4,** 1029–1040
51. Soubeyran, P., Kowanetz, K., Szymkiewicz, I., Langdon, W. Y., and Dikic, I. (2002) *Nature* **416,** 183–187
52. Petrelli, A., Gilestro, G. F., Lanzardo, S., Comoglio, P. M., Migone, N., and Giordano, S. (2002) *Nature* **416,** 187–190

Biochemical and Biophysical Research Communications xxx (2011) xxx–xxx

Contents lists available at ScienceDirect

Biochemical and Biophysical Research Communications

journal homepage: www.elsevier.com/locate/ybbrc

AMSH is required to degrade ubiquitinated proteins in the central nervous system

Shunya Suzuki [a], Keiichi Tamai [a,d,*], Masahiko Watanabe [e], Masanao Kyuuma [a], Masao Ono [c], Kazuo Sugamura [a,d], Nobuyuki Tanaka [b,d]

[a] Department of Microbiology and Immunology, Tohoku University Graduate School of Medicine, Sendai 980-8575, Japan
[b] Department of Cancer Science, Tohoku University Graduate School of Medicine, Sendai 980-8575, Japan
[c] Department of Pathology, Tohoku University Graduate School of Medicine, Sendai 980-8575, Japan
[d] Division of Immunology, Miyagi Cancer Center Research Institute, Natori 981-1293, Japan
[e] Department of Anatomy, Hokkaido University School of Medicine, Sapporo 060-8638, Japan

ARTICLE INFO

Article history:
Received 14 April 2011
Available online xxxx

Keywords:
AMSH
Neurodegeneration
Ubiquitin
Hippocampus

ABSTRACT

Deubiquitination is a biochemical process that mediates the removal of ubiquitin moieties from ubiquitin-conjugated substrates. AMSH (associated molecule with the SH3 domain of STAM) is a deubiquitination enzyme that participates in the endosomal sorting of several cell-surface molecules. AMSH impairment results in missorted ubiquitinated cargoes *in vitro* and severe neurodegeneration *in vivo*, but it is not known how AMSH deficiency causes neuronal damage in the brain. Here, we demonstrate that AMSH$^{-/-}$ mice developed ubiquitinated protein accumulations as early as embryonic day 10 (E10), and that severe deposits were present in the brain at postnatal day 8 (P8) and P18. Interestingly, TDP-43 was found to accumulate and colocalize with glial marker-positive cells in the brain. Glutamate receptor and p62 accumulations were also found; these molecules colocalized with ubiquitinated aggregates in the brain. These data suggest that AMSH plays an important role in degrading ubiquitinated proteins and glutamate receptors *in vivo*. AMSH$^{-/-}$ mice provide an animal model for neurodegenerative diseases, which are commonly characterized by the generation of proteinaceous aggregates.

1. Introduction

The highly dynamic endosomal sorting process determines a membrane-bound protein's fate by either recycling it back to the cell surface or delivering it into endosomal network pathways. Membrane proteins destined for lysosomes are tagged with ubiquitin. Endosomal sorting complexes required for transport (ESCRT) recognizes and dictates cargo selection. ESCRT produces intraluminal vesicles (ILVs) that originate by inward budding from the limiting membrane of the sorting endosome [1]. This process creates a multivesicular body (MVB), which leads to lysosome-dependent cargo degradation through the subsequent MVB-lysosome fusion event.

Balanced ubiquitination and deubiquitination of cargos is a prerequisite for protein homeostasis. Ubiquitin modifications are reversed through the isopeptidase activities of deubiquitinating enzymes (DUBs), with most of the DUBs studied deconjugating only a small number of targets [2]. In fact, deubiquitination, a term used here to refer to both ubiquitin and ubiquitin-like deconjugation, is emerging as a regulatory process in signaling pathways, chromatin structure, endocytosis, and apoptosis [2], and is important for physiological activities such as development, immunity, and neuronal function [3].

We identified AMSH (associated molecule with the SH3 domain of STAM) [4] while screening for an ESCRT-bound molecule. AMSH is an endosomal DUB in the JAMM metalloprotease family, and plays a role in MVB/late endosomes. Recombinant AMSH has been shown to deubiquitinate epidermal growth factor receptor (EGFR) and to cleave lysine 63 (K63)-linked, but not lysine 48 (K48)-linked, polyubiquitin chains into ubiquitin monomers [5]. In a previous study, we found that AMSH binds the ESCRT-III subunit CHMP3 and plays a role in MVB/late endosomes [6]. AMSH also binds the ESCRT-III subunits CHMP1A, CHMP1B, and CHMP2A [7]. This intimate relationship between AMSH and ESCRT prompted us to investigate AMSH's *in vivo* roles. We have reported that AMSH knockout mice (AMSH$^{-/-}$) exhibit postnatal growth retardation and die between postnatal day 19 (P19) and P23. AMSH$^{-/-}$ mice exhibit severe neuronal damage, specifically neuron loss and increasing numbers of apoptotic cells, that is almost en-

Abbreviations: AD, Alzheimer's disease; ALS, amyotrophic lateral sclerosis; AMSH, associated molecule with the SH3 domain of STAM; AMPAR, α-amino-3-hydroxy-5-methyl-isoxazolepropionic acid receptor; CHMP, chromatin modifying protein; ESCRT, endosomal sorting complexes required for transport; FTD, frontotemporal dementia; MVB, multivesicular body; NMDAR, *N*-methyl-D-aspartate receptor; PD, Parkinson's disease; DUB, deubiquitinating enzyme.

* Corresponding author at: Division of Immunology, Miyagi Cancer Center Research Institute, 47-1 Nodayama, Medeshima-Shiode, Natori, Miyagi 981-1293, Japan. Fax: +81 22 381 1168.
E-mail address: tamaikeiichi@mac.com (K. Tamai).

0006-291X/$ - see front matter © 2011 Elsevier Inc. All rights reserved.
doi:10.1016/j.bbrc.2011.04.065

tirely confined to the CA1 subfield of the hippocampus [8]. Despite the severity of these AMSH-deficient neuronal phenotypes, the pathophysiology is not fully understood.

Most age-related neurodegenerative diseases are characterized by accumulations of aberrant protein aggregates in affected regions of the brain. In particular, ubiquitin-positive proteinaceous deposits are a hallmark of neurodegeneration; such deposits include Lewy bodies in Parkinson's disease (PD), neurofibrillary tangles in Alzheimer disease (AD), Bunina bodies in amyotrophic lateral sclerosis (ALS), and Pick bodies in frontotemporal dementia (FTD) with parkinsonism [9]. Since principal function of ubiquitination is to maintain protein homeostasis inside a cell, these neuronal pathologies may indicate a failure to clear unwanted proteins [9]. A recent report suggests that ESCRT-III dysfunction is associated with neurodegeneration resembling age-dependent neurodegenerative diseases such as FTD [10]. A certain percentage of FTD is known as chromosome 3-linked FTD (FTD3), which is attributed to a genetic disorder or mutation of the ESCRT-III molecule CHMP2B [11]. In a previous study using neuron-specific knockout mice, we found that the ESCRT-0 protein Hrs plays a pivotal role in neural cell survival by clearing ubiquitinated proteins in neurons [12]. A growing body of evidence suggests that insufficient ESCRT function leads to the accumulation of ubiquitinated proteins and to human neurodegenerative disease [13]. Nevertheless, little is known about how an ESCRT-associating DUB is involved in ubiquitinated protein degradation in the central nervous system. Here, we demonstrate that ubiquitinated protein accumulations are present in brain lesions found in AMSH$^{-/-}$ mice, and that AMSH is crucial for the proper degradation of both ubiquitinated proteins and glutamate receptors in the central nervous system.

2. Materials and methods

2.1. Cell fractionation

Cerebral tissues were washed with phosphate-buffered saline (PBS), suspended with homogenization buffer (10 mM HEPES, 3 mM imidazole, and 250 mM sucrose), and dissociated by passage through a 22-G needle. The cells were centrifuged at 3000*g* for 10 min at 4 °C, and the supernatants were ultracentrifuged at 100,000*g* for 30 min at 4 °C. The supernatants were regarded as the cytoplasmic fraction, and the pellets as the membrane fraction. The pellets were resuspended with IP buffer (10 mM Hepes, pH 7.2, 0.5% Triton-X, 150 mM NaCl) and centrifuged at 10,000*g* for 30 min at 4 °C. The supernatants were filtered through a polyvinylidene difluoride (PVDF) membrane (0.45 μm, PALL Life Sciences, NY) and regarded as a membrane fraction. These fractions were quantified using the Bio-Rad Protein assay (Bio-Rad, CA) according to the manufacturer's protocol.

2.2. Western blotting

Immunoblotting was conducted as previously described [4]. In brief, mouse brain lysates were fractionated as described above, then separated by sodium dodecyl sulfate–polyacrylamide gel electrophoresis (SDS–PAGE) and transferred onto PVDF membranes (Millipore, MA). After being blocked with 5% nonfat milk in Tris-buffered saline (TBS) containing 0.1% Tween 20, the membranes were probed with the primary antibodies indicated below, washed again, and probed with horseradish peroxidase (HRP)-conjugated secondary antibodies (Cell Signaling, MA).

2.3. Immunofluorescence reactions and immunohistochemistry

For immunofluorescence studies, mice were perfused with 4% paraformaldehyde, and 50-μm sections were prepared using a microslicer (VT1000S, Leica, Nussloch, Germany). The antibodies and dilutions used were as follows: Anti-ubiquitin mouse monoclonal Ab (mAb) 1B3 (MBL, Nagoya, Japan), 1:100; anti-ubiquitin mouse mAb FK2 (BIOMOL, NY), 1:100; anti-TDP-43 mouse mAb (TARDBP) (Proteintech Group, IL), 1:100; anti-p62 (C-terminal specific) guinea pig polyclonal antibody (pAb) (American Research Products, MA), 1:100; anti-GFAP mouse mAb (Chemicon, CA), 1:200; anti-tyrosine hydroxylase rabbit pAb (AB152, Chemicon), 1:1000; anti-microtubule-associated protein 2 goat pAb (MAP2, [14]), 1 μg/mL; anti-calbindin rabbit pAb [15], 1 μg/mL. Appropriately, coupled secondary antibodies (Alexa Fluor, Molecular Probes, CA) were used for double-labeling. For immunohistochemistry, we used the Histofine mouse stain kit or Histofine simple stain mouse MAX-PO(R) (Nichirei, Japan), according to the manufacturer's protocols.

3. Results

Because AMSH is a deubiquitinating enzyme with endosome functions, we analyzed ubiquitinated protein accumulation in the soluble (cytoplasmic) and insoluble (membrane) fractions of the AMSH$^{-/-}$ brain. Western blot analysis using the anti-ubiquitin antibody P4D1 revealed no difference in ubiquitinated protein levels in the soluble fractions from control or AMSH$^{-/-}$ brains (Fig. 1, left panels). In the insoluble fraction, however, the ubiquitinated protein levels were higher in the AMSH$^{-/-}$ brain than in the control (Fig. 1, right panels). The ubiquitinated protein levels in the insoluble fraction increased slightly from embryonic day 10 (E10) to postnatal day 8 (P8) in the control brain, and the levels were higher in the AMSH$^{-/-}$ than the control brain during E10 to P18, near the end of the AMSH$^{-/-}$ mouse lifespan. By P8 the ubiquitinated protein levels in the AMSH$^{-/-}$ brain had increased markedly. These data suggest that AMSH deficiency leads to the progressive accumulation of ubiquitinated proteins in the membrane fraction of the brain.

Histopathological examination of the hippocampus, the brain region most affected in AMSH$^{-/-}$ mice, showed evident neurodegeneration in the CA1 subfield in P6 mice [8]. Confirming the pres-

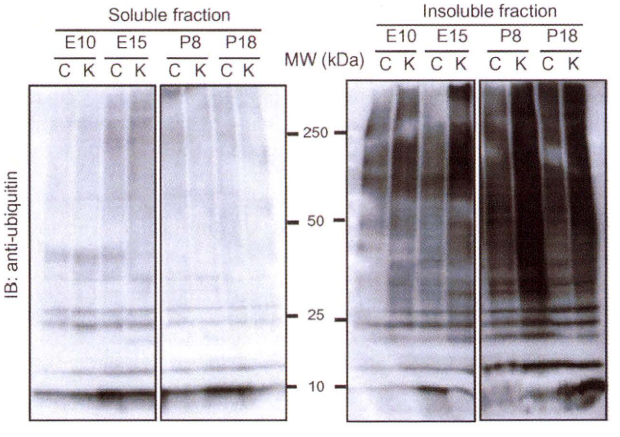

Fig. 1. Ubiquitinated proteins increase with aging in the AMSH knockout mouse brain. Western blots were performed on soluble and insoluble brain fractions of control (C) and AMSH knockout (K) mice at the ages indicated (see Section 2) using the anti-ubiquitin antibody P4D1. Gels were loaded with equal amounts of protein. IB, immunoblotting.

Please cite this article in press as: S. Suzuki et al., AMSH is required to degrade ubiquitinated proteins in the central nervous system, Biochem. Biophys. Res. Commun. (2011), doi:10.1016/j.bbrc.2011.04.065

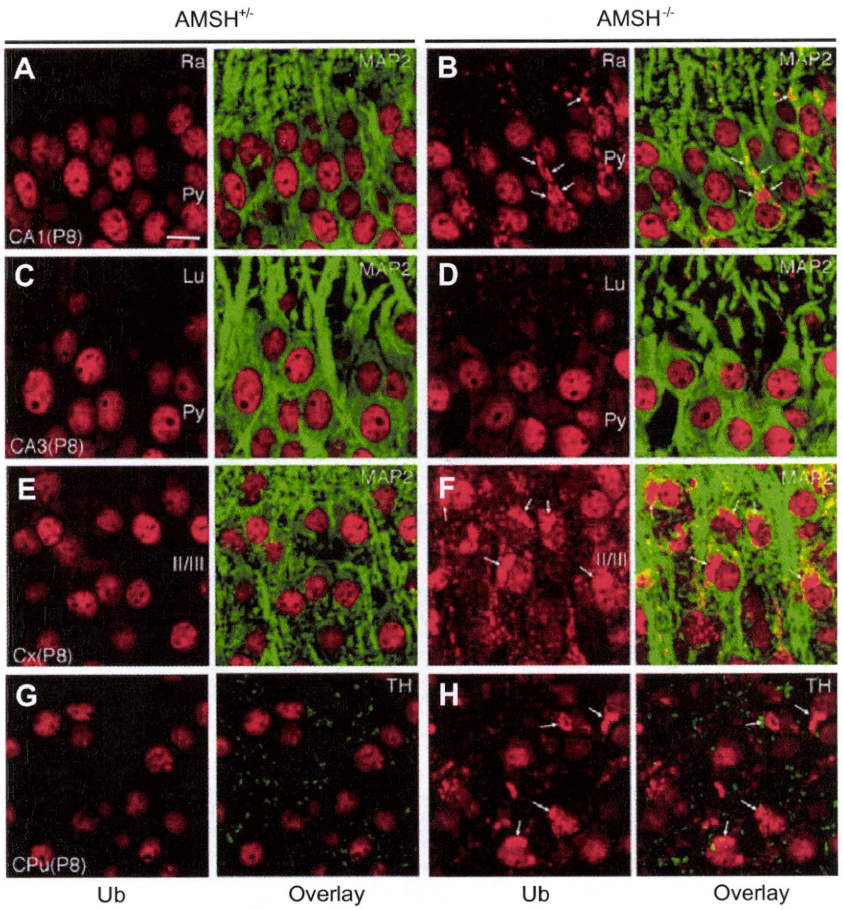

Fig. 2. Ubiquitinated proteins accumulate in the AMSH$^{-/-}$ mouse neurons. Immunofluorescence in postnatal day 8 (P8) AMSH$^{+/-}$ and AMSH$^{-/-}$ tissues stained with antibodies against ubiquitinated proteins in red (clone FK2) is shown in the hippocampal CA1 (A and B), CA3 (C and D), cerebral cortex (E and F), and caudate putamen (G and H). Arrows indicate ubiquitin-positive aggregates. Bar, 10 μm. Lu, stratum lucidum; Py, pyramidal cell layer; Ra, stratum radiatum; II/III, laminae II/III.

ence of neural damage, staining with the glial marker GFAP (glial fibrillary acidic protein) was greater in the hippocampal CA1 subfield of the AMSH$^{-/-}$ P1 brain than in the control, and was profoundly increased in P8 mice (data not shown). To determine whether ubiquitin is involved in the neuronal degeneration observed in AMSH$^{-/-}$ mice, we immunostained brain tissues with FK2, an antibody against ubiquitinated protein. In P8 AMSH$^{-/-}$ brains, FK2-stained granules were clearly apparent in the CA1 subfield, frontal cortex (Cx), and caudate putamen (CPu), but not in the CA3 subfield (Fig. 2A to H in red). The immunostainings of microtubule-associated protein 2 and ubiquitined aggregate were colocalized in CA1 and Cx (Fig. 2A–F). The staining patterns both dopaminergic (tyrosine hydroxylase-positive) fibers in CPu were similar between control and AMSH$^{-/-}$ mice (Fig. 2G and H). The ubiquitinated aggregates in CPu were partially colocalized with dopaminergic fibers, which suggested that ubiquitinated proteins did not accumulated in dopaminergic neurons but in the striatal neurons receiving dopaminergic input. These results suggested that both the ubiquitinated protein accumulation and neuron loss specifically occurred in the AMSH$^{-/-}$ CA1 subfield.

We next examined whether the AMSH deficiency impacts autophagy. Because AMSH is generally known to interact with ESCRT protein components [16], and ESCRT is closely involved with the autophagic pathway [12,17], insufficient autophagy and autophagic protein clearance might account for the aggregation of ubiquitinated proteins in the AMSH$^{-/-}$ mouse brain. We therefore looked at two marker proteins for autophagy: LC3, a specific autophagosome marker, and p62, a ubiquitin-binding protein that is implicated in autophagic protein degradation and that accumulates intracellularly with insufficient autophagy [18]. Although LC3-positive vesicles could not be detected at P20 in either the control or AMSH$^{-/-}$ brain (data not shown), p62 aggregations were clearly observed in pyramidal cell perikarya in the CA1 subfield, Cx, and CPu in the AMSH$^{-/-}$ brain (Fig. 3A and B in red[1] and data not shown). Notably, p62 and ubiquitinated proteins colocalized strongly.

We next examined the expression of the transactivation response element (TAR)-DNA-binding protein 43 (TDP-43), since a previous report suggested that defective ESCRT function leads to aggregations of cytoplasmic proteins, including TDP-43 [19]. Interestingly, TDP-43 was found in several regions of the AMSH$^{-/-}$ P8 brain, including the CA1 subfield, Cx, and CPu (Fig. 3E and F in green and data not shown), and its levels increased markedly from P8 to P20 (Fig. 3G and H). TDP-43 accumulations did not colocalize with ubiquitinated proteins (Fig. 3F), but rather with GFAP (Fig. 3D). These data indicate that TDP-43 accumulates in astrocytes but not neural cells in AMSH$^{-/-}$ mice.

AMSH is known to deubiquitinate receptors, such as the EGF receptor [5] and protease-activated receptor 2 [20], but how AMSH contributes to receptor deubiquitination *in vivo* is unknown. We

[1] For interpretation of color in Figs. 2 and 3, the reader is referred to the web version of this article.

Please cite this article in press as: S. Suzuki et al., AMSH is required to degrade ubiquitinated proteins in the central nervous system, Biochem. Biophys. Res. Commun. (2011), doi:10.1016/j.bbrc.2011.04.065

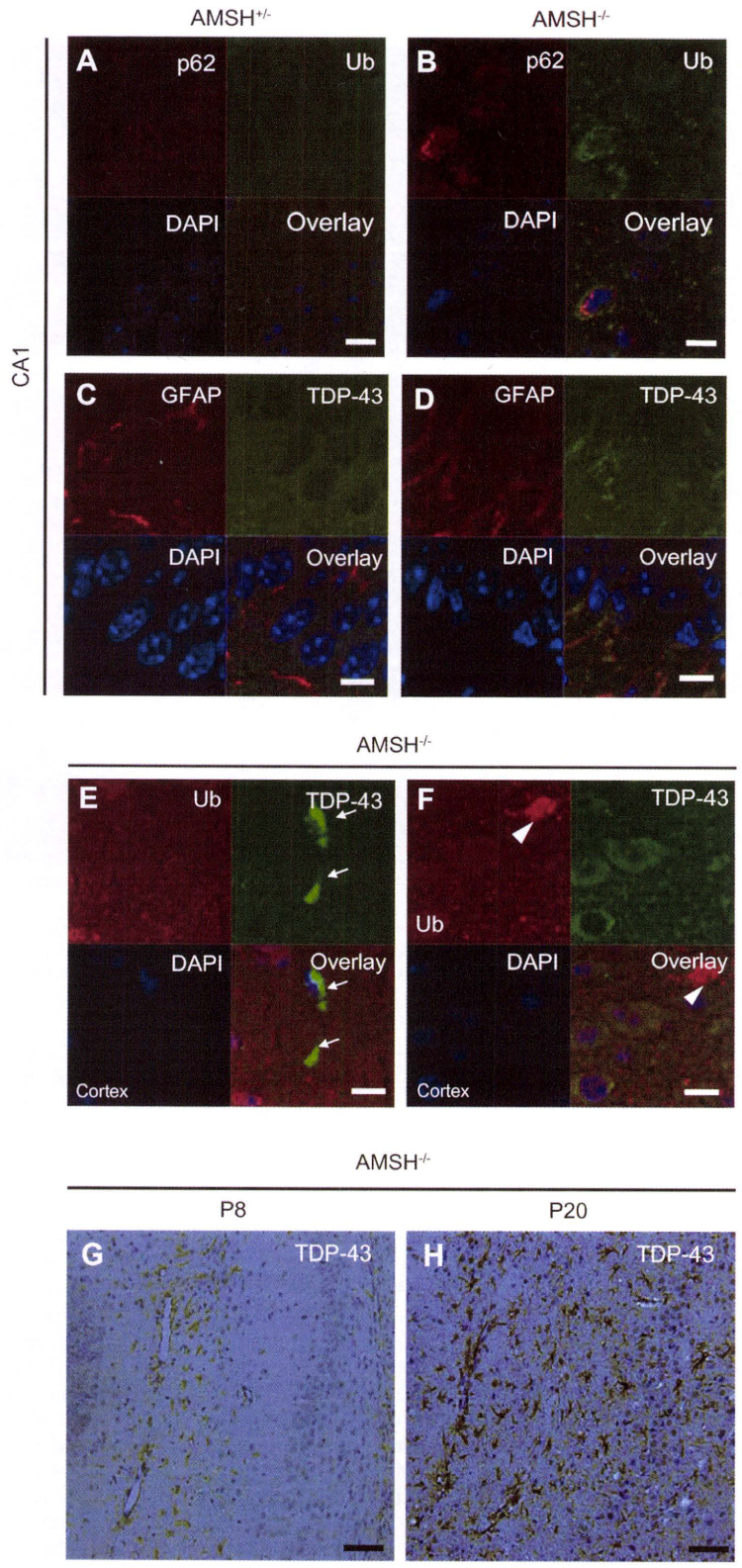

Fig. 3. Ubiquitinated proteins, p62, and TDP-43 accumulate in the AMSH$^{-/-}$ mouse brain. (A and B) Immunofluorescence in P20 AMSH$^{+/-}$ and AMSH$^{-/-}$ tissues stained with antibodies against ubiquitinated proteins (1B3) and p62 is shown in the hippocampal CA1. (C and D) TDP-43 and GFAP colocalize in the AMSH$^{-/-}$ mouse brain. Immunofluorescence staining with antibodies against GFAP and TDP-43 in AMSH$^{+/-}$ and AMSH$^{-/-}$ mice at P20 in the hippocampal CA1 subfield. Bar, 10 μm. (E and F) Immunofluorescence staining in the cerebral cortex of P20 AMSH$^{+/-}$ and AMSH$^{-/-}$ mice, using antibodies against ubiquitinated proteins (1B3) and TDP-43. Arrows indicate TDP-43-positive cells. Arrowheads indicate ubiquitin-positive cells. Bar, 10 μm. (G and H) Immunohistochemistry of hippocampal CA1 subfields from AMSH$^{-/-}$ mice at P8 (E) and P20 (F), stained with an anti-TDP-43 antibody. Bar, 50 μm.

Please cite this article in press as: S. Suzuki et al., AMSH is required to degrade ubiquitinated proteins in the central nervous system, Biochem. Biophys. Res. Commun. (2011), doi:10.1016/j.bbrc.2011.04.065

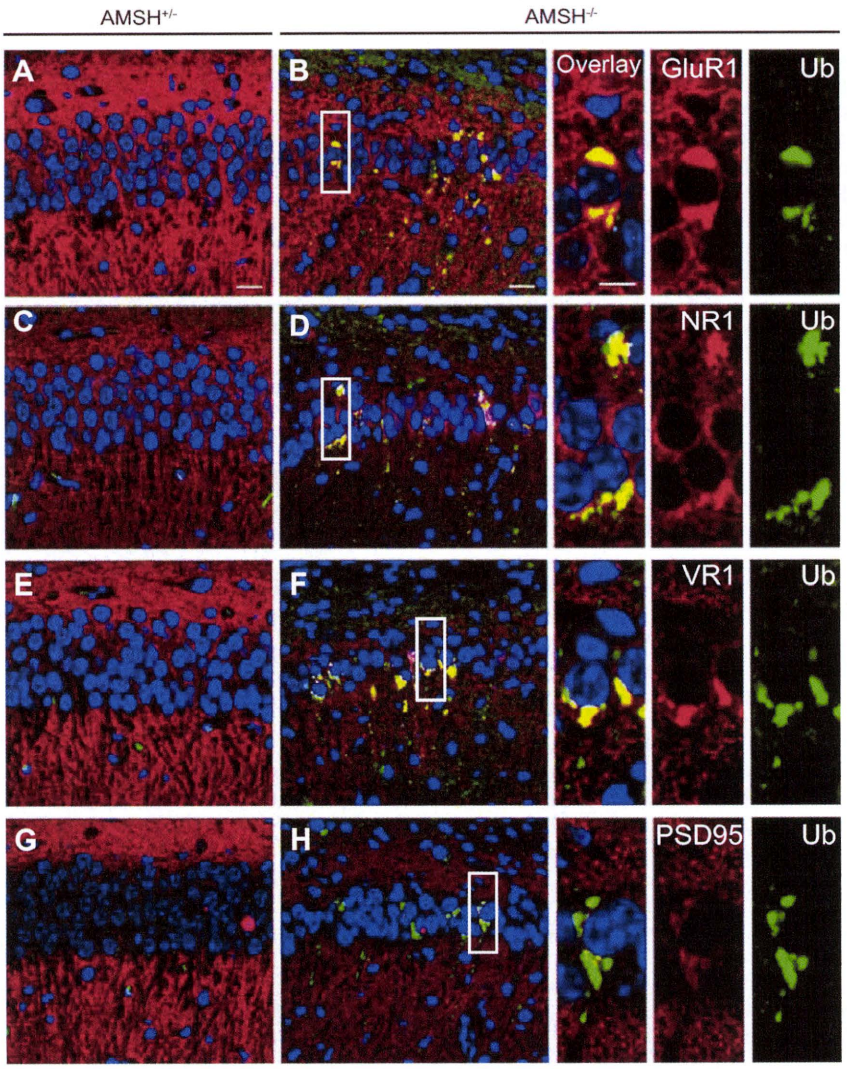

Fig. 4. Patterns of glutamate receptor subunits and ubiquitinated proteins. Immunofluorescence reactions in P8 AMSH$^{+/-}$ (A, C, E, G) and AMSH$^{-/-}$ (B, D, F, H) mice are shown. CA1 subfields were counterstained with DAPI (blue) and stained with antibodies (red) against GluR1 (A and B), NR1 (C and D), VR1 (E and F), and PSD95 (G and H). Ubiquitinated proteins were also stained in green.

suspected that glutamate receptors, which play prominent roles in several neurodegenerative diseases [21], might be regulated by AMSH. We used immunohistochemistry to examine the expression and localization of GluR1, which is a subunit of the α-amino-3-hydroxy-5-methyl-isoxazolepropionic acid receptor (AMPAR), as well as NR1 and VR1, which are subunits of the *N*-methyl-D-aspartate receptor (NMDAR), in the CA1 subfield. Aggregates in the AMSH$^{+/-}$ brain were not stained by antibodies against GluR1, NR1, or VR1 (Fig. 4A, C, E, and G); however, glutamate receptor-positive aggregates were clearly visible (Fig. 4B, D, F, and H). PSD95, which is known to bind Hrs and control glutaminergic synapse function, was weakly detected and was found colocalized with ubiquitinated proteins. Interestingly, we found the colocalization of glutamate receptor- and ubiquitin-positive aggregates (Fig. 4B, D, F, and H, insets). These results indicate that AMSH is critical for glutamate receptor regulation.

4. Discussion

The present study demonstrated that ubiquitinated proteins were accumulated in the membranous fractions of the AMSH-deficient mouse brain, indicating that membrane traffic is altered. These accumulations were found as early as E10. In a previous study, we found neuron loss in the AMSH-deficient CA1 subfield on and after P8, but not at E19 or P1 [8]. Ubiquitinated protein aggregates in neurons are known to induce neurodegeneration in conditions such as AD, FTD, and ALS [9]. Therefore, it is reasonable that we detected aggregates of ubiquitinated proteins prior to neurodegeneration in the AMSH-deficient brain. Ubiquitinated proteinaceous aggregates in the brains of AMSH-knockout mice colocalized with p62, which also accumulates in the affected neurons. The protein p62 binds ubiquitin and the autophagosome marker protein LC3, and regulates aggregate formation [22]. In addition, p62 is a selective target of autophagy, and is eventually degraded in lysosomes as a result of the autophagosome-lysosome fusion event [22]. Based on these findings, it is possible that AMSH is required for the basal or naturally occurring autophagic clearance of aggregate-prone proteins by facilitating the autophagosome-lysosome fusion.

We also observed TDP-43 aggregates in GFAP-positive glial cells in the AMSH-deficient brain, and these aggregates were not stained by anti-ubiquitin antibodies. In contrast, TDP-43 has been

Please cite this article in press as: S. Suzuki et al., AMSH is required to degrade ubiquitinated proteins in the central nervous system, Biochem. Biophys. Res. Commun. (2011), doi:10.1016/j.bbrc.2011.04.065

reported to accumulate in cytoplasmic lesions in neural cells and to colocalize with ubiquitin-positive cellular inclusions in human neurodegenerative diseases such as ALS and FTD [23]. However, a recent study showed that neuronal and glial inclusions were positively stained with ubiquitin and TDP-43 antibodies in some FTD brain specimens [24]. As TDP-43 is known to be polyubiquitinated in the presence of proteasome inhibitors [25], we expected AMSH to be critical for degrading TDP-43 in glial cells. However, we failed to detect TDP-43 ubiquitination in glial cells. Furthermore, we also examined alpha-synuclein, one of the proteins affected in PD, and phosphorylated Tau, which accumulates in AD, and found no differences between the $AMSH^{+/-}$ and $AMSH^{-/-}$ brains (data not shown). These results suggest that there may be an unknown substrate that needs to be cleared by AMSH-dependent deubiquitination and sorting, or that AMSH may be required for non-specific clearance of unwanted proteins. Further study is required to find AMSH substrates related to neurodegenerative disease.

In contrast to our present findings of neurodegeneration in the CA1 subfield in AMSH knockout mice, we previously reported finding CA3 sector neurodegeneration in STAM1-knockout as well as neuron-specific Hrs-knockout mice [12,26]. STAM1 and Hrs form an ESCRT-0 complex, which sorts ubiquitinated proteins upstream of ESCRT-III [27]. The mechanism determining the specificity of neurodegeneration in CA1 versus CA3 is an intriguing issue. Since AMSH and Hrs are distributed ubiquitously in the hippocampus, including the CA1 and CA3 subfields [8,12], their expression patterns do not account for the difference. The glutamate receptor subunit aggregates that we found in the CA1 subfield of the $AMSH^{-/-}$ brain in this study have also been found in the CA3 subfield in the Hrs-knockout brain. While we cannot completely exclude the possibility that neurodegeneration itself causes the accumulations of ubiquitinated aggregates, we suspect that instead, neurodegeneration is a result of impaired glutamate receptor regulation; we found that ubiquitinated protein accumulations were already present at E10 and E15 in the $AMSH^{-/-}$ brain, before CA1 pyramidal neuron loss occurs [8]. We also suspect that the survival of hippocampal neurons in the CA1 and CA3 subfields requires novel, distinct proteins that are subject to ubiquitination. Further study is required to determine how endosomal trafficking is regulated in the different subfields in the hippocampus.

Among the ESCRT molecules, CHMP2B mutations cause chromosome 3-linked, familial FTD (FTD-3) in humans. CHMP2B is a component of ESCRT-III, and like AMSH, is recruited to the endosomes and MVB for cargo sorting. Because AMSH binds indirectly with CHMP2B via another ESCRT-III molecule, CHMP3 [28], AMSH depletion and CHMP2B mutations seem to share similar pathological features. Indeed, neurodegeneration in FTD-3 patients is distributed not only in the frontal, parietal and temporal cortex, but also in the hippocampus. Histopathological changes found in patients with late stages of ubiquitin-positive FTD include changes in the CA1 sector of the hippocampus [29]. In addition, p62 and ubiquitinated protein accumulations are related to human neurodegenerative diseases [18]. It is not known whether AMSH selectively recognizes harmful gene products associated with neurodegenerative disorders. However, AMSH mutant mice provide an excellent animal model system for studying the molecular mechanisms of neurodegenerative diseases.

Acknowledgments

This work was supported by JSPS and MEXT KAKENHI (21590517, 19059001, and 22790630), by a Grant-in-Aid from the Ministry of Health, Labor and Welfare, by Takeda Medical Research Foundation, and by Intelligent Cosmos Research Institute.

References

[1] J.H. Hurley, S.D. Emr, The ESCRT complexes: structure and mechanism of a membrane-trafficking network, Annu. Rev. Biophys. Biomol. Struct. 35 (2006) 277–298.
[2] S.M. Nijman, M.P. Luna-Vargas, A. Velds, T.R. Brummelkamp, A.M. Dirac, T.K. Sixma, R. Bernards, A genomic and functional inventory of deubiquitinating enzymes, Cell 123 (2005) 773–786.
[3] P.C. Evans, Regulation of pro-inflammatory signalling networks by ubiquitin: identification of novel targets for anti-inflammatory drugs, Expert Rev. Mol. Med. 7 (2005) 1–19.
[4] N. Tanaka, K. Kaneko, H. Asao, H. Kasai, Y. Endo, T. Fujita, T. Takeshita, K. Sugamura, Possible involvement of a novel STAM-associated molecule "AMSH" in intracellular signal transduction mediated by cytokines, J. Biol. Chem. 274 (1999) 19129–19135.
[5] J. McCullough, M.J. Clague, S. Urbe, AMSH is an endosome-associated ubiquitin isopeptidase, J. Cell Biol. 166 (2004) 487–492.
[6] M. Kyuuma, K. Kikuchi, K. Kojima, Y. Sugawara, M. Sato, N. Mano, J. Goto, T. Takeshita, A. Yamamoto, K. Sugamura, N. Tanaka, AMSH, an ESCRT-III associated enzyme, deubiquitinates cargo on MVB/late endosomes, Cell Struct. Funct. 31 (2007) 159–172.
[7] M. Agromayor, J. Martin-Serrano, Interaction of AMSH with ESCRT-III and deubiquitination of endosomal cargo, J. Biol. Chem. 281 (2006) 23083–23091.
[8] N. Ishii, Y. Owada, M. Yamada, S. Miura, K. Murata, H. Asao, H. Kondo, K. Sugamura, Loss of neurons in the hippocampus and cerebral cortex of AMSH-deficient mice, Mol. Cell. Biol. 21 (2001) 8626–8637.
[9] C.A. Ross, M.A. Poirier, Protein aggregation and neurodegenerative disease, Nat. Med. 10 (Suppl.) (2004) S10–S17.
[10] J.A. Lee, A. Beigneux, S.T. Ahmad, S.G. Young, F.B. Gao, ESCRT-III dysfunction causes autophagosome accumulation and neurodegeneration, Curr. Biol. 17 (2007) 1561–1567.
[11] G. Skibinski, N.J. Parkinson, J.M. Brown, L. Chakrabarti, S.L. Lloyd, H. Hummerich, J.E. Nielsen, J.R. Hodges, M.G. Spillantini, T. Thusgaard, S. Brandner, A. Brun, M.N. Rossor, A. Gade, P. Johannsen, S.A. Sorensen, S. Gydesen, E.M. Fisher, J. Collinge, Mutations in the endosomal ESCRTIII-complex subunit CHMP2B in frontotemporal dementia, Nat. Genet. 37 (2005) 806–808.
[12] K. Tamai, M. Toyoshima, N. Tanaka, N. Yamamoto, Y. Owada, H. Kiyonari, K. Murata, Y. Ueno, M. Ono, T. Shimosegawa, N. Yaegashi, M. Watanabe, K. Sugamura, Loss of hrs in the central nervous system causes accumulation of ubiquitinated proteins and neurodegeneration, Am. J. Pathol. 173 (2008) 1806–1817.
[13] C. Raiborg, H. Stenmark, The ESCRT machinery in endosomal sorting of ubiquitylated membrane proteins, Nature 458 (2009) 445–452.
[14] E. Miura, M. Fukaya, T. Sato, K. Sugihara, M. Asano, K. Yoshioka, M. Watanabe, Expression and distribution of JNK/SAPK-associated scaffold protein JSAP1 in developing and adult mouse brain, J. Neurochem. 97 (2006) 1431–1446.
[15] S. Nakagawa, M. Watanabe, T. Isobe, H. Kondo, Y. Inoue, Cytological compartmentalization in the staggerer cerebellum, as revealed by calbindin immunohistochemistry for Purkinje cells, J. Comp. Neurol. 395 (1998) 112–120.
[16] M.J. Clague, S. Urbe, Endocytosis: the DUB version, Trends Cell Biol. 16 (2006) 551–559.
[17] M. Filimonenko, S. Stuffers, C. Raiborg, A. Yamamoto, L. Malerod, E.M. Fisher, A. Isaacs, A. Brech, H. Stenmark, A. Simonsen, Functional multivesicular bodies are required for autophagic clearance of protein aggregates associated with neurodegenerative disease, J. Cell Biol. 179 (2007) 485–500.
[18] M. Komatsu, S. Waguri, M. Koike, Y.S. Sou, T. Ueno, T. Hara, N. Mizushima, J. Iwata, J. Ezaki, S. Murata, J. Hamazaki, Y. Nishito, S. Iemura, T. Natsume, T. Yanagawa, J. Uwayama, E. Warabi, H. Yoshida, T. Ishii, A. Kobayashi, M. Yamamoto, Z. Yue, Y. Uchiyama, E. Kominami, K. Tanaka, Homeostatic levels of p62 control cytoplasmic inclusion body formation in autophagy-deficient mice, Cell 131 (2007) 1149–1163.
[19] T.E. Rusten, A. Simonsen, ESCRT functions in autophagy and associated disease, Cell Cycle 7 (2008) 1166–1172.
[20] B. Hasdemir, J.E. Murphy, G.S. Cottrell, N.W. Bunnett, Endosomal deubiquitinating enzymes control ubiquitination and down-regulation of protease-activated receptor 2, J. Biol. Chem. 284 (2009) 28453–28466.
[21] T.M. Tzschentke, Glutamatergic mechanisms in different disease states: overview and therapeutical implications – an introduction, Amino Acids 23 (2002) 147–152.
[22] S. Pankiv, T.H. Clausen, T. Lamark, A. Brech, J.A. Bruun, H. Outzen, A. Overvatn, G. Bjorkoy, T. Johansen, P62/SQSTM1 binds directly to Atg8/LC3 to facilitate degradation of ubiquitinated protein aggregates by autophagy, J. Biol. Chem. 282 (2007) 24131–24145.
[23] F. Geser, M. Martinez-Lage, L.K. Kwong, V.M. Lee, J.Q. Trojanowski, Amyotrophic lateral sclerosis, frontotemporal dementia and beyond: the TDP-43 diseases, J. Neurol. 256 (2009) 1205–1214.
[24] N.J. Cairns, M. Neumann, E.H. Bigio, I.E. Holm, D. Troost, K.J. Hatanpaa, C. Foong, C.L. White 3rd, J.A. Schneider, H.A. Kretzschmar, D. Carter, L. Taylor-Reinwald, K. Paulsmeyer, J. Strider, M. Gitcho, A.M. Goate, J.C. Morris, M. Mishra, L.K. Kwong, A. Stieber, Y. Xu, M.S. Forman, J.Q. Trojanowski, V.M. Lee, I.R. Mackenzie, TDP-43 in familial and sporadic frontotemporal lobar degeneration with ubiquitin inclusions, Am. J. Pathol. 171 (2007) 227–240.

Please cite this article in press as: S. Suzuki et al., AMSH is required to degrade ubiquitinated proteins in the central nervous system, Biochem. Biophys. Res. Commun. (2011), doi:10.1016/j.bbrc.2011.04.065

[25] M.J. Winton, L.M. Igaz, M.M. Wong, L.K. Kwong, J.Q. Trojanowski, V.M. Lee, Disturbance of nuclear and cytoplasmic TAR DNA-binding protein (TDP-43) induces disease-like redistribution, sequestration, and aggregate formation, J. Biol. Chem. 283 (2008) 13302–13309.
[26] M. Yamada, T. Takeshita, S. Miura, K. Murata, Y. Kimura, N. Ishii, M. Nose, H. Sakagami, H. Kondo, F. Tashiro, J.I. Miyazaki, H. Sasaki, K. Sugamura, Loss of hippocampal CA3 pyramidal neurons in mice lacking STAM1, Mol. Cell. Biol. 21 (2001) 3807–3819.
[27] Y. Tanaka, N. Tanaka, Y. Saeki, K. Tanaka, M. Murakami, T. Hirano, N. Ishii, K. Sugamura, C-Cbl-dependent monoubiquitination and lysosomal degradation of gp130, Mol. Cell. Biol. 28 (2008) 4805–4818.
[28] B. McDonald, J. Martin-Serrano, No strings attached: the ESCRT machinery in viral budding and cytokinesis, J. Cell Sci. 122 (2009) 2167–2177.
[29] C. Kersaitis, G.M. Halliday, J.J. Kril, Regional and cellular pathology in frontotemporal dementia: relationship to stage of disease in cases with and without Pick bodies, Acta Neuropathol. 108 (2004) 515–523.

Please cite this article in press as: S. Suzuki et al., AMSH is required to degrade ubiquitinated proteins in the central nervous system, Biochem. Biophys. Res. Commun. (2011), doi:10.1016/j.bbrc.2011.04.065

J Gastroenterol (2011) 46:232–241
DOI 10.1007/s00535-010-0297-2

ORIGINAL ARTICLE—LIVER, PANCREAS, AND BILIARY TRACT

Lymphotropic HCV strain can infect human primary naïve CD4$^+$ cells and affect their proliferation and IFN-γ secretion activity

Yasuteru Kondo · Yoshiyuki Ueno · Eiji Kakazu · Koju Kobayashi · Masaaki Shiina · Keiichi Tamai · Keigo Machida · Jun Inoue · Yuta Wakui · Koji Fukushima · Noriyuki Obara · Osamu Kimura · Tooru Shimosegawa

Received: 9 May 2010 / Accepted: 11 July 2010 / Published online: 17 August 2010

Abstract
Background Lymphotropic hepatitis C virus (HCV) infection of B and T cells might play an important role in the pathogenesis of hepatitis C. Recently, we showed that a lymphotropic HCV (SB strain) could infect established T-cell lines and B-cell lines. However, whether HCV replication interferes with cell proliferation and function in primary T lymphocytes is still unclear.
Aim The aim of this study was to analyze whether HCV replication in primary T lymphocytes affected their development, proliferation, and Th1 commitment.
Methods SB strain cell culture supernatant (2×10^4 copies/ml HCV) was used to infect several kinds of primary lymphocyte subsets. Mock, UV-irradiated SB-HCV, JFH-1 strain, and JFH-1 NS5B mutant, which could not replicate in T cells, were included as negative controls. Carboxyfluorescein succinimidyl ester (CFSE) and CD45RA double staining was used to evaluate the proliferative activity of CD4$^+$CD45RA$^+$CD45RO$^-$ naïve CD4$^+$ cells. Interferon (IFN)-γ and interleukin (IL)-10 secretion assays magnetic cell sorting (MACS) were carried out.
Results Negative strand HCV RNA was detected in CD4$^+$, CD14$^+$, and CD19$^+$ cells. Among CD4$^+$ cells, CD4$^+$CD45RA$^+$RO$^-$ cells (naïve CD4$^+$ cells) were most susceptible to replication of the SB strain. The levels of CFSE and CD45RA expression gradually declined during cell division in uninfected cells, while HCV-infected naïve CD4$^+$ cells expressed higher levels of CFSE and CD45RA than Mock or UV-SB infected naïve CD4$^+$ cells. Moreover, the production of IFN-γ was significantly suppressed in SB-infected naïve CD4$^+$ cells.
Conclusions Lymphotropic HCV replication suppressed proliferation and development, including that towards Th1 commitment, in human primary naïve CD4$^+$ cells.

Keywords HCV · Lymphotropic · Naïve CD4$^+$ cell · Th1

Electronic supplementary material The online version of this article (doi:10.1007/s00535-010-0297-2) contains supplementary material, which is available to authorized users.

Y. Kondo · Y. Ueno (✉) · E. Kakazu · M. Shiina · K. Tamai · J. Inoue · Y. Wakui · K. Fukushima · N. Obara · O. Kimura · T. Shimosegawa
Division of Gastroenterology,
Tohoku University Graduate School of Medicine,
1-1 Seiryo, Aobaku, Sendai 980-8574, Japan
e-mail: yueno@med.tohoku.ac.jp

K. Machida
Department of Molecular Microbiology and Immunology,
University of Southern California Keck School of Medicine,
2011 Zonal Avenue, Los Angeles, CA 90033, USA

K. Kobayashi
School of Health Science, Tohoku University, 1-1 Seiryo,
Aobaku, Sendai 980-8574, Japan

Introduction

Hepatitis C virus (HCV) infects about 170 million people worldwide and is a major cause of chronic hepatitis, liver cirrhosis, and hepatocellular carcinoma (HCC) [1]. Cellular and humoral immune responses to HCV play an important role in the pathogenesis of chronic hepatitis, liver cirrhosis, HCC, and B-lymphocyte proliferative disorders, including mixed cryoglobulinemia, a disorder characterized by the oligoclonal proliferation of B cells [2, 3].

Several mechanisms have been proposed for the failure of the cellular immune response, including anergy, cytotoxic T-lymphocyte (CTL) exhaustion, suppression via

regulatory $CD4^+$–$CD25^+$ T cells interleukin-10 (IL-10)-secreting regulatory $CD8^+$-T cells, and direct binding of HCV core antigen [4–7]. However, the influence of HCV replication in lymphoid cells on their functions is not fully understood. HCV replicates primarily in the liver, but HCV-RNA has been detected in other lymphoid cells, including B- and T-lymphocytes, monocytes, and dendritic cells [8–11]. Sung et al. [12] have previously reported a B-cell line (SB cells) that produces HCV particles that can further infect B lymphocytes in vitro. We have shown that the SB-HCV strain could infect and replicate in T-cell lines and that HCV replication could inhibit interferon (IFN)-γ/signal transducer and activator of transcription-1 (STAT-1)/T-bet signaling of the T cells [13]. Moreover, we reported that HCV replication in Molt-4 could affect the proliferation and FAS-mediated apoptosis of T cells by inhibiting CD44v6 expression and mitogen-activated protein kinase (MAPK) signaling in Molt-4 [14]. Most of these data came from studies using cell lines, since stable SB-HCV replication could be detected in lymphoid cell lines (Raji, Molt-4, etc.). However, the analysis of primary lymphocytes is preferable to determine the real effects of lymphotropic HCV strains on T-cell biology. In fact, the effects of low titers of HCV in primary T cells have not been clarified yet.

We first reported that, among T cells, $CD4^+CD45RA^+RO^-$ naïve T cells were susceptible to SB-HCV infection [13]. Here we describe the functional and proliferative analysis of SB-HCV-infected naïve $CD4^+$ T cells after short-term culture.

Materials and methods

Culture of cell lines

SB cells that continuously produce infectious HCV particles were originally established from splenocytes of an HCV-infected patient with type 2 mixed cryoglobulinemia and monocytoid B-cell lymphoma [12]. The cells were maintained in standard RPMI (Invitrogen, Carlsbad, CA, USA) medium with 20% fetal bovine serum (FBS) without any supplement. Every 5 days, the cells were sedimented by natural gravity for 30 min at 37°C.

In vitro infection of primary lymphoid cells

Supernatants from SB cells were purified by centrifugation and 0.2-μm filter. SB culture supernatant (5 ml), which contained 2.2×10^4 copies/ml of HCV RNA, was used for the infection of several kinds of human primary lymphoid cells (1×10^5 cells). A control infection with UV-irradiated SB culture supernatant was included in every experiment. Supernatants of Huh7.5 cells transfected with JFH-1 strains [15–17] at 10 days post-transfection were used for several control experiments. Cells were washed 3 times at 2 days after infection. Then, a portion of the cells (3×10^5 to 5×10^5 cells) was harvested for analysis; the remaining cells (1×10^5 cells) were kept and incubated under the same condition.

Isolation of various kinds of lymphoid cells and naïve $CD4^+$ T cells

We got informed consent from 5 healthy donors, from whom peripheral blood mononuclear cells (PBMC) were isolated by Ficoll-Paque centrifugation (Amersham Bioscience [Uppsala, Sweden]). Anti-CD3 phycoerythrin (PE), anti-CD4 (PE-Cy3), anti-CD8 (PE), anti-CD14 (PE), anti-CD19 (PE), anti-CD45RO (PE), and antiCD45RA (fluorescein isothiocyanate [FITC]) antibodies (BD Pharmingen) were used for the separation of different kinds of mononuclear cells by using fluorescence activated cell sorting (FACS) vantage (BD Parmingen, San Jose, CA, USA). In some experiments, a naïve $CD4^+$ T cell isolation kit II (Miltenyi Biotec [Bergish Gladbach, Germany]) was used to obtain more viable naïve $CD4^+$ cells.

Strand-specific intracellular HCV RNA detection

Strand-specific intracellular HCV RNA was detected by using a recently established procedure that combined previously published methods [9, 18] with minor modifications [13]. Positive- and negative-strand-specific HCV RNAs were detected by a nested polymerase chain reaction (PCR) method. Reactions were performed with 2 μl of 10× reverse transcriptase (RT) buffer, 2 μl of 10-mmol/l magnesium chloride, 200-μmol/l each of deoxyadenosine triphosphate, deoxycytidine triphosphate, deoxyguanosine triphosphate, 100-μmol/l of thymidine triphosphate (dTTP), 0.2 U of uracil-*N* glycosylase (UNG; Perkin Elmer [Fremount, CA, USA]/Applied Biosystems), 5 U of rTth DNA Polymerase; and 50 pmol of strand-specific HCV primers (positions according to the 5′ untranslated region), nt −285 to −256 (ACTGTCTTCACGCAGAAAGCGTCT AGCCAT) and −43 to −14 (CGAGACCTCCCGGGGCA CTCGCAAGCACCC) and template RNA. The RT mixture was incubated for 10 min at room temperature and then at 70°C for an additional 15 min. The cDNA product was subjected to the first PCR with 80 μl of PCR reaction buffer containing 50 pmol of HCV downstream strand-specific primer. The PCR amplification consisted of 5 min at 95°C, followed by 35 cycles (1 min at 94°C, followed by 1 min at 67°C, and then by 1 min at 72°C), and then 7-min extension at 72°C. For the second nested PCR, an aliquot (1/10) of the first PCR reaction mixture was re-amplified

using 50 pmol of each of the two primers, nt −276 to −247 (ACGCAGAAAGCGTCTAGCCATGGCGTTAGT) and nt −21 to −50 (TCCCGGGGCACTCGCAAGCACCCT ATCAGG), which span the 255-base pair region nt −276 to −21 (position according to the 5′ untranslated region) of HCV RNA, and Taq polymerase (Applied Biosystems). The reaction was run for 35 cycles (1 min at 94°C, 1 min at 67°C, 1 min at 72°C), followed by 7 min at 72°C. Semi-quantification was achieved by serial fourfold dilutions (in 10 μg/ml of *Escherichia coli* tRNA) of an initial amount of 200 ng of total RNA. The relative titer was expressed as the highest dilution giving a visible band of the appropriate size on a 2% agarose gel stained by ethidium bromide. For internal control, semi-quantification of β-actin mRNA was performed by using the same RNA extracts. To rule out false, random, and self-priming, extracted HCV RNA was run in every RT–PCR test without the addition of an upstream HCV primer.

CFSE staining

Cells were analyzed by using a CellTrace CFSE Cell Proliferation Kit (Invitrogen [Carlsbad, CA, USA]). The cell staining methods followed the manufacturer's protocol. Stained cells were washed three times and incubated for an additional 7 days. Cells were analyzed by flow cytometry with 510 nm excitation and emission filters. A proliferation index was calculated by FlowJo 7.5 (Tree Str Inc, Ashland, OR, USA), according to the manufacturer's protocol.

Annexin V and propidium iodide staining

Cells were stained with Annexin V and propidium iodide (PI) by using an apoptosis detection kit (R&D systems, Minneapolis, MN, USA). Staining methods were conducted according to the manufacturer's protocol. Briefly, collected cells were washed and gently re-suspended in the Annexin V incubation reagent at a concentration of 3×10^5 cells per 100 μl. Then, re-suspended cells in binding buffer were stained by Streptavidin conjugate allophycocyanin (APC) and analyzed by flow cytometry within 1 h.

Transfection of HCV individual protein expression plasmids

The various expression plasmids were constructed by inserting HCV core, E1, E2, NS3, NS4B, NS5A, and NS5B cDNA of genotype 1a [19] behind the cytomegalovirus virus immediate-early promoter in pCDNA3.1 (Invitrogen). Primary $CD4^+$ cells were transfected using Nucleofector I (Amaxa, Gaithersburg, Washington DC, USA) with a Human T cell Nucleofector kit (Amaxa), and various plasmids were purified using the EndFree plasmid kit (QIAGEN, Valencia, CA, USA). Viable transfected cells were isolated by Ficoll-Paque centrifugation (Amersham Bioscience) at 24 h post-transfection. Transfection and expression efficiency were analyzed by using intracellular staining of HCV individual proteins and flow cytometry analysis. Briefly, the cells were fixed and permeabilized with fixation/permeabilization solution (BD Bioscience) at 4°C for 25 min. The cells were then washed two times in BD Perm/Wash buffer (BD Bioscience) and resuspended in 50 μl of BD Perm/Wash buffer containing pre-conjugating polyclonal anti-E1, E2, NS3, NS4B, NS5B, NS5A antibody (abcam, Cambridge, MA, USA) with a phycoerythrin (PE)-conjugated anti-mouse antibody.

Confocal laser microscopy

Primary lymphocytes (3×10^6 cells/ml) in suspension were fixed and permeabilized with fixation/permeabilization solution (BD Bioscience) at 4°C for 25 min. The cells were then washed two times in BD Perm/Wash buffer (BD Bioscience) and resuspended in 50 μl of BD Perm/Wash buffer containing pre-conjugating polyclonal anti-NS5A antibody (Biodesign International, Saco, ME, USA) with an FITC-conjugated anti-mouse antibody.

Interferon-γ and interleukin 10 secretion assay

Cells were washed by adding 2 ml of cold phosphate-buffered saline (PBS) and resuspended in 90 μl of cold RPMI 1640 medium. After the addition of 10 μl of IL-10- or IFN-γ-Catch Reagent (Miltenyi Biotec), cells were incubated for 5 min on ice. Then the cells were diluted with 1 ml of warm medium (37°C) and further incubated in a closed tube for 45 min at 37°C under slow continuous rotation. Cells were washed and IL-10- or IFN-γ-secreting cells were stained by adding 10 μL of IL-10- or IFN-γ-detection antibody (PE-conjugated) (Miltenyi Biotec) together with anti-CD4-PerCP.

Real-time PCR analysis

Cells were collected sequentially at various time points after the addition of recombinant human IFN-γ (500 ng/ml) (BD Biosciences, CA, USA). After the extraction of total RNA and the RT procedure, real-time PCR using a TaqMan Chemistry System was carried out. The ready-made set of primers and probe for the amplification of T-bet (ID HS00203436) and glyceraldehyde-3-phosphate-dehydrogenase (GAPDH) were purchased from Perkin-Elmer/Applied Biosystems. The relative amount of target mRNA was obtained by using a comparative the threshold cycle (CT) method. The expression level of mRNAs of the non-stimulation sample of vector transfected-primary

$CD4^+$ cells was represented as 1.0 and the relative amount of target mRNA in a stimulated sample was calculated according to the manufacturer's protocol.

Immunoblot assay

Proteins were resolved by electrophoresis in sodium dodecyl sulfate–polyacrylamide gels and electrophoretically transferred onto a polyvinylidene difluoride (PVDF) membrane (Bio-Rad, Hercules, CA, USA). The membrane was incubated with anti-STAT-1α, or anti-p-STAT-1 antibodies (Cell Signaling, Danver, MA, USA) and then reacted with peroxidase-conjugated secondary antibody. Immunoreactivity was visualized by an enhanced chemiluminescence detection system (Amersham Bioscience).

Statistical analysis

Statistical analyses of the data in Figs. 1c, 2c, 3b, and 4 were performed by the analysis of variance (ANOVA)

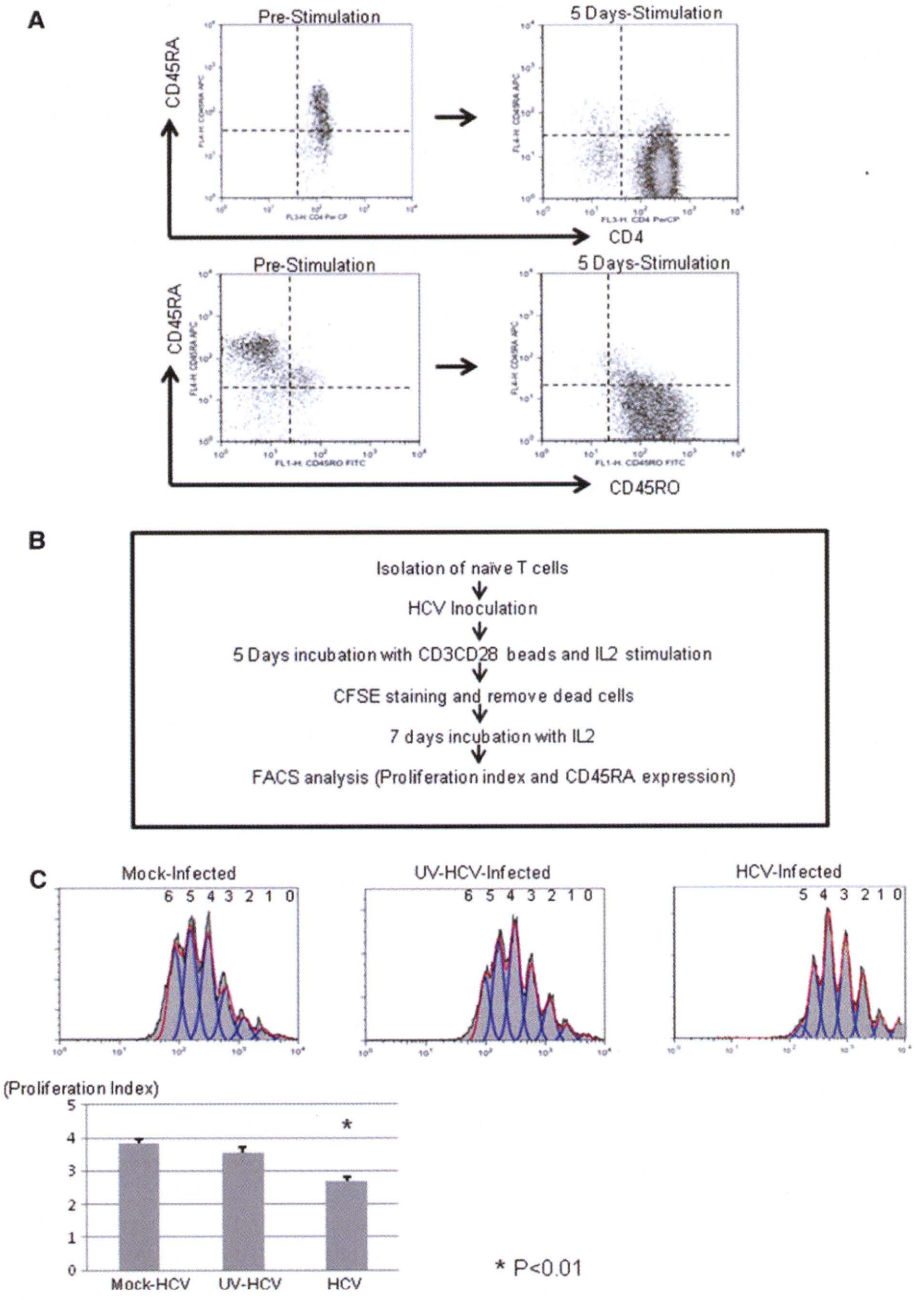

Fig. 1 Suppression of proliferation activity in hepatitis C virus (*HCV*)-infected human naïve T lymphocytes. **a** A representative dot plot of $CD4^+CD45RA^+RO^-$ cells is shown. Cells are stained with CD4-PerCP-antibody (Ab), CD45RA-fluorescein isothiocyanate (FITC)-Ab, and CD45RO-APC-Ab. The purity of isolated $CD4^+CD45RA^+RO^-$ naïve T lymphocytes is over 92%. **b**, **c** Carboxyfluorescein succinimidyl ester (CFSE) staining was carried out at 5 days post-infection in SB-HCV, UV-irradiated HCV, and Mock. Stained cells were washed three times and incubated for an additional 7 days with T-cell expander. Cells were analyzed by flow cytometry with 510 nm excitation and emission filters. *Numbers* in the representative histogram indicate numbers of cell divisions. The proliferation index was calculated by FlowJo 7.5 software according to the manufacturer's protocol. The proliferation index is shown in this *bar graph*. Three independent experiments were carried out. *Error bars* indicate the standard deviation. *IL* interleukin

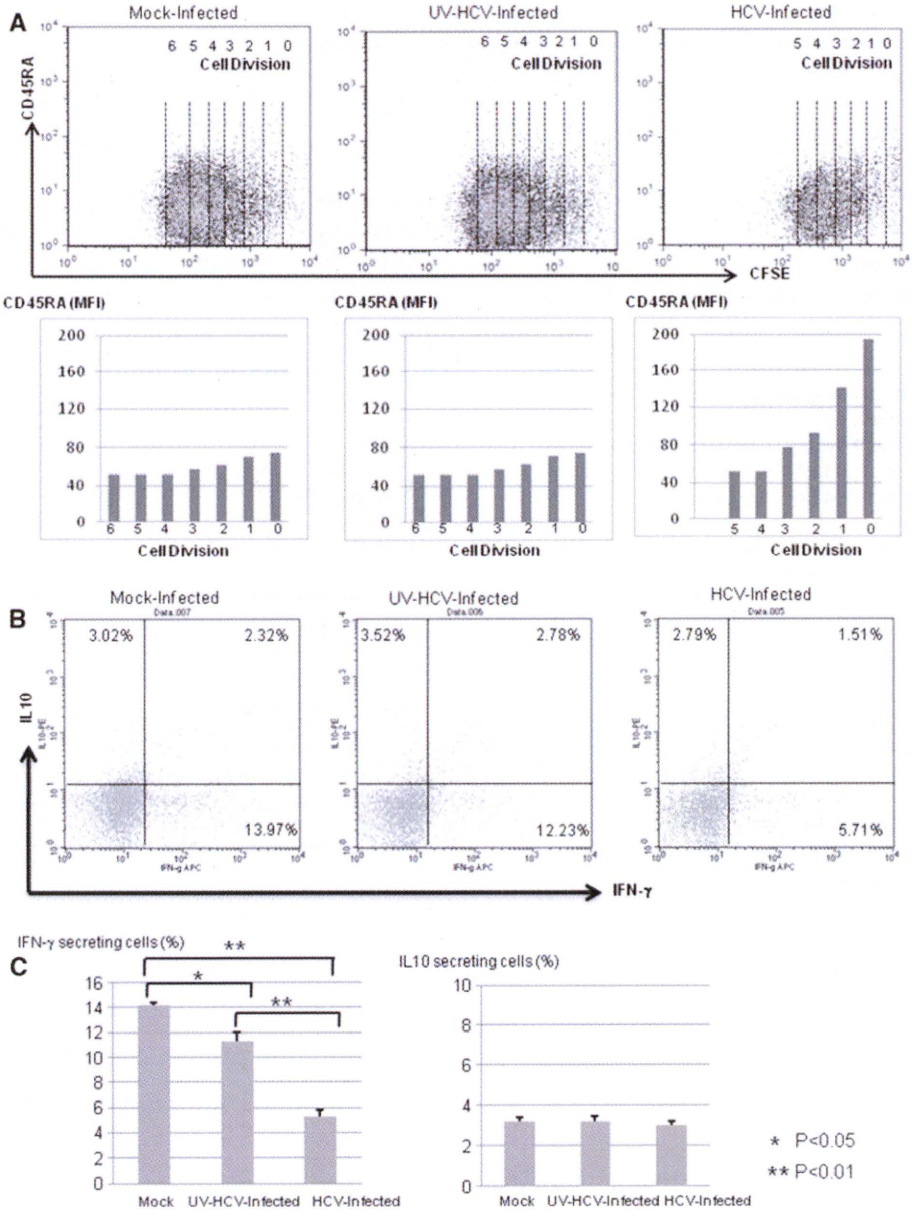

Fig. 2 Suppression of development and Th1 commitment in HCV-infected human naïve T lymphocytes. **a** Representative dot plots of CD45RA and carboxyfluorescein succinimidyl ester (CFSE) double staining are shown. *Numbers* in the representative dot plots indicate the numbers of cell divisions. *Bar graphs* indicate the mean fluorescence intensity (MFI) of cell clusters. **b** Representative dot plots of interferon-γ (*IFN-γ*) and interleukin (IL) 10 secretion assays are shown. The *numbers* in the quadrant indicate IFN-γ and/or IL10-secreting cells among $CD4^+$ cells. **c** The frequencies of IFN-γ- and IL10-secreting cells among the three groups are shown in these *bar graphs*. Three independent experiments were carried out. *Error bars* indicate the standard deviation

test (SPSS10.0, SPSS Inc, Chicago, IL, USA). Values of $p < 0.05$ were considered to be statistically significant.

Results

Detection of negative-strand HCV-RNA among lymphoid cells

Strand-specific rTth based nested PCR was carried out to analyze the susceptibility to HCV infection among the various kinds of lymphoid cells with or without short term culture (7 days). Isolated lymphoid cells were infected with SB-HCV, UV-irradiated-HCV, or JFH-1 strain and were cultured with appropriate cytokines and/or antibody stimulation (Table 1). We needed to add different kinds of cytokines to maintain the cell proliferation and viability. Negative-strand HCV-RNA could be detected in $CD4^+$, $CD14^+$, and $CD19^+$ cells and in $CD8^+$ cell-depleted PBMCs (PBMC-$CD8^+$) after short-term culture (Table 2). However, negative- and positive-strand HCV-RNA could not be detected in any kinds of lymphoid cells infected with the supernatant of JFH-1 and JFH-1 GND mutant (data not shown). Undetectable negative-strand HCV-RNA at 2 days post-infection indicated that HCV-RNA was replicated after inoculation. We found that depletion of $CD8^+$ cells from

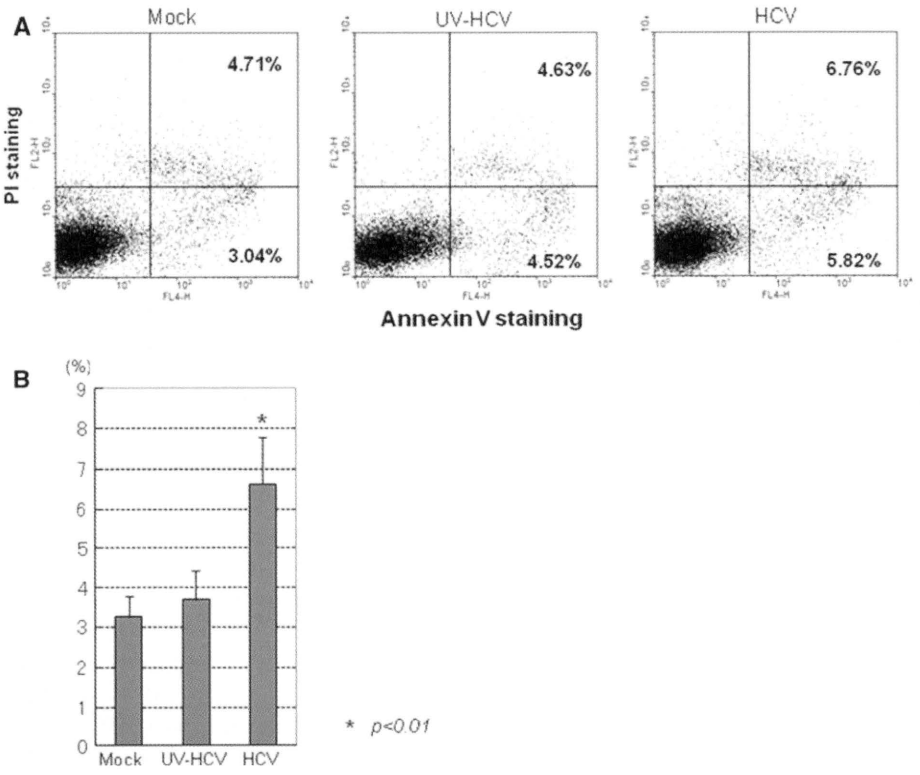

Fig. 3 HCV replication induces apoptosis of naive $CD4^+$ cells. **a** Representative dot plots of Annexin V and propidium iodide (*PI*) staining are shown. The *numbers* in the quadrants indicate the frequencies of early apoptotic cells (Annexin V^+ and PI^-) and dead cells (Annexin V^+ and PI^+ cells). **b** The frequencies of early apoptotic cells are shown in this *bar graph*. Three independent experiments were carried out. *Error bars* indicate the standard deviations

PBMCs was favorable to replication in lymphoid cells. In this study, we used CD3CD28 beads and IL2 stimulation that could stimulate more efficiently than CD3 and IL2 stimulation. However, among the $CD4^+$ cells, $CD4^+$ $CD45RA^+RO^-$ naïve $CD4^+$ cells were most susceptible to infection, as we previously demonstrated (Table 2) (Suppl. Fig. 1) [13]. These data indicate that $CD4^+CD45RA^+RO^-$ naïve $CD4^+$ cells could be infected with SB-HCV during T-cell development. CD81 was one of the main candidates of HCV receptors for the infection of the cells [20–22]. We tried to analyze whether anti-CD81 antibody might block the SB-HCV infection of primarily naïve $CD4^+$ cells. HCV-NS5A protein could be detected in 12.2% of SB-HCV-inoculated naïve $CD4^+$ cells at 10 days post-infection. However, the pretreatment of anti-CD81 antibody reduced the frequency of NS5A detection among the SB-HCV-inoculated naïve $CD4^+$ cells (4.7%) (Suppl. Fig. 2). The sensitivity of NS5A immunostaining was lower than that of the strand-specific nested PCR method [13].

Suppression of proliferation activity in SB-HCV-infected naïve $CD4^+$ cells

The purity of $CD45RA^+RO^-$ naïve $CD4^+$ cells after isolation was around 92% (Fig. 1a). CFSE staining was carried out at 5 days post-infection in SB-HCV, UV-irradiated HCV, and Mock. Stained cells were washed three times and incubated for an additional 7 days with T-cell expander (CD3CD28 coated beads and IL2 stimulation). Cells were analyzed by flow cytometry with 510 nm excitation and emission filters. The proliferation index was calculated by FlowJo 7.5 software according to the manufacturer's protocol. The proliferation index of SB-HCV-infected naïve $CD4^+$ cells was significantly lower than that of controls ($p < 0.01$) (Fig. 1b, c). These data indicate that lymphotropic SB-HCV suppresses the proliferation activity of T cells.

Disturbance of cell development and IFN-γ-secreting activity

CD45RA and CFSE double staining was carried out to analyze the cell development. The expression level of CD45RA on naïve $CD4^+$ cells had gradually declined during cell proliferation. However, the CD45RA expression level of SB-HCV-infected naïve $CD4^+$ cells remained higher than those of the control groups (Fig. 2a). Moreover, the frequency of IFN-γ-secreting cells among SB-HCV-infected $CD4^+$ cells was significantly lower than those of the control groups ($p < 0.01$) (Fig. 2b, c). On the other hand, the frequency of IL10-secreting cells was comparable in the three groups (Fig. 2b, c). These data indicate that HCV infection could interrupt cell development, especially Th1 development.

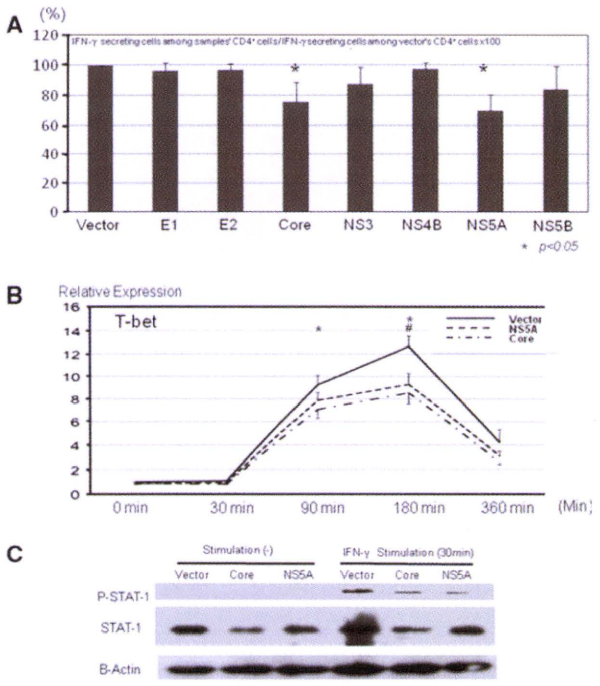

Fig. 4 HCV-Core and NS5A proteins are the proteins that contribute to the suppression of IFN-γ secretion. **a** HCV E1, E2, Core, NS3, NS4B, NS5A, and NS5B expression plasmids were used to transfect into primary $CD4^+$ lymphocytes by Nucleofector. The frequencies of IFN-γ-secreting cells among the samples' $CD4^+$ cells/the frequencies of IFN-γ-secreting cells among the vector's $CD4^+$ cells $\times 100$ are shown in this *bar graph*. **b** HCV core and NS5A transfected primary $CD4^+$ lymphocytes were stimulated with IFN-γ (500 ng/ml). The relative expression of T-bet-mRNA was sequentially analyzed by real-time polymerase chain reaction (PCR). The relative amount of target mRNA was obtained by using a comparative the threshold cycle (CT) method. The expression level of mRNAs of the nonstimulation sample of vector transfected-primary $CD4^+$ cells is represented as 1.0 and the relative amount of target mRNA in a stimulated sample was calculated. Three independent experiments were carried out. *Error bars* indicate the standard deviation. **c** Immunoblotting assay was carried out to detect the protein of signal transducer and activator of transcription-1 (*STAT-1*), phospho-STAT-1 (*p-STAT-1*), and actin in the HCV-core, NS5A, and vector-plasmid transfected human primary $CD4^+$ cells with or without IFN-γ stimulation (30 min)

SB-HCV infection could induce apoptosis of naïve $CD4^+$ cells

Annexin V and PI double staining were carried out to detect early apoptotic cells. The frequency of Annexin-V-positive PI-negative early apoptotic cells in SB-HCV-infected naïve T cells was significantly higher than those in the control groups ($p < 0.01$) (Fig. 3a, b). UV-irradiated SB-HCV did not enhance the induction of apoptosis in naïve T cells with CD3CD28 stimulation. During T-cell activation, apoptosis is easily induced in order to maintain an appropriate immune response. In line with this feature, 3.04% of early apoptotic cells were detected in naïve T cells with CD3CD28 beads stimulation and Mock serum. These data indicate that SB-HCV replication could induce apoptosis, as seen in Molt-4 cells [14].

HCV core and NS5A proteins could suppress IFN-γ secretion from primary $CD4^+$ cells

We investigated the HCV proteins responsible for the suppression of IFN-γ secretion. HCV E1, E2, Core, NS3, NS4B, NS5A, and NS5B expression plasmids were used to transfect into primary $CD4^+$ lymphocytes by Nucleofector. The intracellular staining of these proteins was carried out and the transfection efficiency was about 35–55% (Suppl. Fig. 3). Among these proteins, HCV core and NS5A could significantly suppress the IFN-γ secretion ($p < 0.05$) (Fig. 4). HCV core and NS5A transfected primary $CD4^+$ lymphocytes were stimulated with IFN-γ. The relative expression of T-bet-mRNA was sequentially analyzed by real-time PCR. T-bet-mRNA expression in HCV core or NS5A transfected primary $CD4^+$ T lymphocytes was significantly suppressed at 90 and 180 min post-transfection in comparison to vector-transfected primary $CD4^+$ T lymphocytes. Moreover, the amount of STAT-1 protein in HCV-Core-expressing $CD4^+$ cells was remarkably lower than the amounts in vector and HCV-E2 transfected $CD4^+$ cells

Table 1 Cytokine conditions for various kinds of lymphoid cell culture

Cells	Cytokine condition	Other stimulant	Cell viability (%)
PBMC	IL2 (50 ng/ml) + IL6 (20 ng/ml) + CSF (250 ng/ml)	None	80
PBMC-CD8	IL2 (50 ng/ml) + IL6 (20 ng/ml) + CSF (250 ng/ml)	None	80
CD3	IL2 (50 ng/ml)	CD3CD28 coated beads	70
CD4	IL2 (50 ng/ml)	CD3CD28 coated beads	70
CD8	IL2 (50 ng/ml)	CD3CD28 coated beads	70
CD14	CSF (250 ng/ml)	None	60
CD19	IL-6 (20 ng/ml)	None	70

The conditions of the cell culture are shown. Peripheral blood mononuclear cell (PBMC)-CD8 indicates CD8 cell-depleted PBMCs

IL interleukin, *CSF* colony stimulating factor

Table 2 Strand-specific hepatitis C virus (HCV)-RNA detection in various kinds of lymphoid cells

Subset	PBMC	PBMC-CD8	CD3	CD4	CD8	CD14	CD19
Positive strand							
2 days	+	+	−	+	−	−	+
7 days	++	++	+	++	−	++	+++
7 days UV-irradiated	−	−	−	−	−	−	−
Negative strand							
2 days	−	−	−	−	−	−	−
7 days	−	+	+/−	+	−	+	++
7 days UV-irradiated	−	−	−	−	−	−	−

Subset	Whole $CD4^+$	$CD4^+CD45RA^+RO^-$	$CD4^+CD45RA^-RO^+$
Positive strand			
2 days	+	+	+
7 days	++	+++	+
7 days UV-irradiated	−	−	−
Negative strand			
2 days	−	−	−
7 days	+	++	+/−
7 days UV-irradiated	−	−	−

Positive- and negative-strand-specific HCV-RNA was detected by semiquantitative nested polymerase chain reaction (PCR) methods

−, negative detection; +, positive detection without dilution; ++, positive detection with 4 times dilution; +++, positive detection with 16 times dilution; ±, only one detection in three independent experiments. Three independent experiments were carried out. Similar results were obtained three times

(Fig. 4c). The amount of phosphorylated STAT-1 (p-STAT-1) after IFN-γ stimulation was also analyzed. The amount of p-STAT-1 in HCV-Core and NS5A expressing $CD4^+$ cells was remarkably lower than that in the vector control.

Discussion

There are many reports about the existence of extrahepatic HCV replication that might contribute to immune dysfunction [13, 14, 23–25]. We have reported that a specific SB-HCV strain could replicate in B- and T-cell lines and affect various immune systems [13, 14, 25]. However, the results of these studies were not definitely conclusive, since the cell lines were inappropriate to investigate the development and commitment of the lymphocytes. In the present study, we demonstrated that the SB-HCV strain could replicate in primary $CD19^+$ B cells, $CD4^+$ T cells, and $CD14^+$ monocytes with cytokine stimulation. Among the $CD4^+$ T cells, $CD4^+CD45RA^+RO^-$ naïve $CD4^+$ cells were the most susceptible to SB-HCV infection. One of the speculated reasons to explain why naïve $CD4^+$ cells with stimulation were most susceptible to SB-HCV infection is that T cells might temporarily express various kinds of molecules which may contribute to the HCV infection during T-cell development. The infectivity of naïve $CD4^+$ T cells was not as high as that of Molt-4 cells. However, significant suppression of cell development and IFN-γ secretion were seen in SB-HCV-infected naïve T cells with CD3, CD28, and IL2 stimulation. UV-irradiated-HCV that could not replicate in the cells suppressed the IFN-γ secretion slightly. These data indicate that not only the effect of HCV replication but also the direct binding effects of HCV structured proteins might contribute to the suppression of IFN-γ secretion. One report indicated that HCV-core protein could interact with the complement receptor gC1qR and upregulate suppressor of cytokine signaling-1 (SOCS-1), accompanied by downregulation of signal transducer and activator of transcription-1 (STAT-1) phosphorylation in T cells [7]. Another possible explanation of the discrepancies between HCV infectivity and suppression of proliferation and IFN-γ secretion might be the low sensitivity of HCV antigen-immunostaining, since lower sensitivity of immunostaining in comparison to the nested PCR method was found in our previous study [13].

HCV-Core and -NS5A proteins were the proteins responsible for the suppression of IFN-γ secretion from T cells. Lin et al. [26] have documented that HCV-core protein causes the degradation of STAT-1 protein and suppresses the Jak-STAT pathway in hepatocytes. In our previous study, reduction of STAT-1 protein was detected in HCV-core transfected primary naïve T cells and HCV-replicating Molt-4 cells [13]. Moreover, inhibition of intrahepatic gamma interferon production by HCV-NS5A

in transgenic mice was recently reported [27]. Recently, detection of HCV replicative intermediate RNA in perihepatic lymph nodes was reported [28]. The disturbance of Th1 commitment might influence the development of HCV-specific CTL in perihepatic lymph nodes. The selective infection of certain T cells by HCV in vivo may explain why there is only relative HCV-specific T-cell suppression without general immune suppression.

Suppression of proliferation activity was seen in HCV-infected naïve T cells as well as HCV-infected Molt-4 cells [14]. The expression level of CD45RA, which is a surface marker of T-cell development, gradually declined along with cell proliferation. However, HCV-infected naïve T cells expressed significantly higher levels of CD45RA than the control groups. We previously reported that HCV replication could suppress Ras/MEK/ERK signaling of Molt-4 [14]. During T-cell development, T cells showed strong proliferation activity that might facilitate HCV replication in T cells. However, extensive proliferation of HCV in T cells might interfere with the proper development of T cells.

The induction of apoptosis was seen in SB-HCV-infected naive T lymphocytes with CD3CD28 and IL2 stimulation. It is known that, during T-cell activation from naïve to effector cells, T cells have to survive activation-induced cell death (AICD), which may contribute to the maintenance of an appropriate level of the immune response [29, 30]. However, some groups reported that HCV replication could inhibit apoptosis in hepatoma cell lines [31, 32]. The developmental stages and characteristics of naïve T cells might explain these contradictory results. During T-cell activation, apoptosis is easily induced in order to maintain an appropriate immune response.

In conclusion, HCV replication in human naïve T cells might affect their proliferation activity and Th1 development, as was shown in the cell lines used in a previous study. The results suggest that the infectivity of HCV in human naïve T lymphocytes is low, although the biological effect of this infection might be significant because of its bystander effects.

Acknowledgments This work was supported in part by a Grant-in-Aid from the Ministry of Education, Culture, Sport, Science, and Technology of Japan (#21790642 to Y.K.), and by Health and Labour Sciences Research Grants for Research on Measures for Intractable Diseases (from the Ministry of Health, Labour and Welfare of Japan (to Y.U.). We are grateful to Dr. Michael M.C. Lai for providing the SB-HCV strain, and to Dr. Takaji Wakita for providing pJFH-1 and pJFH-1/GND.

References

1. Alter MJ, Kruszon-Moran D, Nainan OV, McQuillan GM, Gao F, Moyer LA, et al. The prevalence of hepatitis C virus infection in the United States, 1988 through 1994. N Engl J Med. 1999; 341(8):556–62.
2. Chang KM, Rehermann B, Chisari FV. Immunopathology of hepatitis C. Springer Semin Immunopathol. 1997;19(1):57–68.
3. Ferri C, Caracciolo F, Zignego AL, La Civita L, Monti M, Longombardo G, et al. Hepatitis C virus infection in patients with non-Hodgkin's lymphoma. Br J Haematol. 1994;88(2):392–4.
4. Accapezzato D, Francavilla V, Paroli M, Casciaro M, Chircu LV, Cividini A, et al. Hepatic expansion of a virus-specific regulatory CD8(+) T cell population in chronic hepatitis C virus infection. J Clin Invest. 2004;113(7):963–72.
5. Manigold T, Racanelli V. T-cell regulation by CD4 regulatory T cells during hepatitis B and C virus infections: facts and controversies. Lancet Infect Dis. 2007;7(12):804–13.
6. Blackburn SD, Wherry EJ. IL-10, T cell exhaustion and viral persistence. Trends Microbiol. 2007;15(4):143–6.
7. Yao ZQ, Prayther D, Trabue C, Dong ZP, Moorman J. Differential regulation of SOCS-1 signalling in B and T lymphocytes by hepatitis C virus core protein. Immunology. 2008; 125(2):197–207.
8. Bare P, Massud I, Parodi C, Belmonte L, Garcia G, Nebel MC, et al. Continuous release of hepatitis C virus (HCV) by peripheral blood mononuclear cells and B-lymphoblastoid cell-line cultures derived from HCV-infected patients. J Gen Virol. 2005; 86(Pt 6):1717–27.
9. Hu Y, Shahidi A, Park S, Guilfoyle D, Hirshfield I. Detection of extrahepatic hepatitis C virus replication by a novel, highly sensitive, single-tube nested polymerase chain reaction. Am J Clin Pathol. 2003;119(1):95–100.
10. Laporte J, Bain C, Maurel P, Inchauspe G, Agut H, Cahour A. Differential distribution and internal translation efficiency of hepatitis C virus quasi species present in dendritic and liver cells. Blood. 2003;101(1):52–7.
11. Li Y, Wang X, Douglas SD, Metzger DS, Woody G, Zhang T, et al. CD8+ T cell depletion amplifies hepatitis C virus replication in peripheral blood mononuclear cells. J Infect Dis. 2005;192(6):1093–101.
12. Sung VM, Shimodaira S, Doughty AL, Picchio GR, Can H, Yen TS, et al. Establishment of B-cell lymphoma cell lines persistently infected with hepatitis C virus in vivo and in vitro: the apoptotic effects of virus infection. J Virol. 2003;77(3):2134–46.
13. Kondo Y, Sung VM, Machida K, Liu M, Lai MM. Hepatitis C virus infects T cells and affects interferon-gamma signaling in T cell lines. Virology. 2007;361(1):161–73.
14. Kondo Y, Machida K, Liu HM, Ueno Y, Kobayashi K, Wakita T, et al. Hepatitis C virus infection of T cells inhibits proliferation and enhances fas-mediated apoptosis by down-regulating the expression of CD44 splicing variant 6. J Infect Dis. 2009; 199(5):726–36.
15. Lindenbach BD, Evans MJ, Syder AJ, Wolk B, Tellinghuisen TL, Liu CC, et al. Complete replication of hepatitis C virus in cell culture. Science. 2005;309(5734):623–6.
16. Wakita T, Pietschmann T, Kato T, Date T, Miyamoto M, Zhao Z, et al. Production of infectious hepatitis C virus in tissue culture from a cloned viral genome. Nat Med. 2005;11(7):791–6.
17. Kato T, Date T, Murayama A, Morikawa K, Akazawa D, Wakita T. Cell culture and infection system for hepatitis C virus. Nat Protoc. 2006;1(5):2334–9.
18. Negro F, Krawczynski K, Quadri R, Rubbia-Brandt L, Mondelli M, Zarski JP, et al. Detection of genomic- and minus-strand of hepatitis C virus RNA in the liver of chronic hepatitis C patients by strand-specific semiquantitative reverse-transcriptase polymerase chain reaction. Hepatology. 1999;29(2):536–42.
19. Machida K, Cheng KT, Sung VM, Lee KJ, Levine AM, Lai MM. Hepatitis C virus infection activates the immunologic (type II) isoform of nitric oxide synthase and thereby enhances DNA

damage and mutations of cellular genes. J Virol. 2004;78(16): 8835–43.
20. Harris HJ, Farquhar MJ, Mee CJ, Davis C, Reynolds GM, Jennings A, et al. CD81 and claudin 1 coreceptor association: role in hepatitis C virus entry. J Virol. 2008;82(10):5007–20.
21. Molina S, Castet V, Pichard-Garcia L, Wychowski C, Meurs E, Pascussi JM, et al. Serum-derived hepatitis C virus infection of primary human hepatocytes is tetraspanin CD81 dependent. J Virol. 2008;82(1):569–74.
22. Cormier EG, Tsamis F, Kajumo F, Durso RJ, Gardner JP, Dragic T. CD81 is an entry coreceptor for hepatitis C virus. Proc Natl Acad Sci USA. 2004;101(19):7270–4.
23. Kanto T, Inoue M, Miyatake H, Sato A, Sakakibara M, Yakushijin T, et al. Reduced numbers and impaired ability of myeloid and plasmacytoid dendritic cells to polarize T helper cells in chronic hepatitis C virus infection. J Infect Dis. 2004; 190(11):1919–26.
24. Kanto T, Hayashi N, Takehara T, Tatsumi T, Kuzushita N, Ito A, et al. Impaired allostimulatory capacity of peripheral blood dendritic cells recovered from hepatitis C virus-infected individuals. J Immunol. 1999;162(9):5584–91.
25. Machida K, Kondo Y, Huang JY, Chen YC, Cheng KT, Keck Z, et al. Hepatitis C virus (HCV)-induced immunoglobulin hypermutation reduces the affinity and neutralizing activities of antibodies against HCV envelope protein. J Virol. 2008;82(13): 6711–20.
26. Lin W, Choe WH, Hiasa Y, Kamegaya Y, Blackard JT, Schmidt EV, et al. Hepatitis C virus expression suppresses interferon signaling by degrading STAT1. Gastroenterology. 2005;128(4): 1034–41.
27. Kanda T, Steele R, Ray R, Ray RB. Inhibition of intrahepatic gamma interferon production by hepatitis C virus nonstructural protein 5A in transgenic mice. J Virol. 2009;83(17):8463–9.
28. Pal S, Sullivan DG, Kim S, Lai KK, Kae J, Cotler SJ, et al. Productive replication of hepatitis C virus in perihepatic lymph nodes in vivo: implications of HCV lymphotropism. Gastroenterology. 2006;130(4):1107–16.
29. Krammer PH. CD95's deadly mission in the immune system. Nature. 2000;407(6805):789–95.
30. Holmstrom TH, Schmitz I, Soderstrom TS, Poukkula M, Johnson VL, Chow SC, et al. MAPK/ERK signaling in activated T cells inhibits CD95/Fas-mediated apoptosis downstream of DISC assembly. EMBO J. 2000;19(20):5418–28.
31. Nanda SK, Herion D, Liang TJ. The SH3 binding motif of HCV [corrected] NS5A protein interacts with Bin1 and is important for apoptosis and infectivity. Gastroenterology. 2006;130(3):794–809.
32. Miyasaka Y, Enomoto N, Kurosaki M, Sakamoto N, Kanazawa N, Kohashi T, et al. Hepatitis C virus nonstructural protein 5A inhibits tumor necrosis factor-alpha-mediated apoptosis in Huh7 cells. J Infect Dis. 2003;188(10):1537–44.